

# Merging Structural Motifs of Functionalized Amino Acids and $\alpha$ -Aminoamides Results in Novel Anticonvulsant Compounds with Significant Effects on Slow and Fast Inactivation of Voltage-Gated Sodium Channels and in the Treatment of Neuropathic Pain

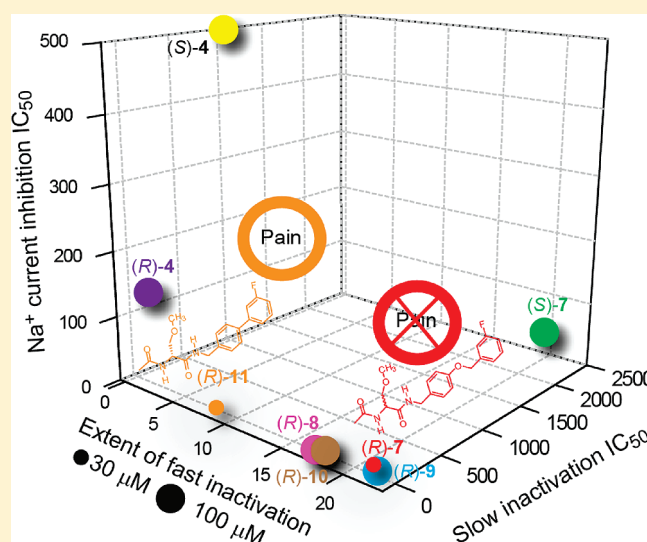
Yuying Wang,<sup>†</sup> Sarah M. Wilson,<sup>#,§</sup> Joel M. Brittain,<sup>#,§</sup> Matthew S. Ripsch,<sup>‡,§</sup> Christophe Salomé,<sup>‡</sup> Ki Duk Park,<sup>‡</sup> Fletcher A. White,<sup>‡,§</sup> Rajesh Khanna,<sup>\*,†,§</sup> and Harold Kohn<sup>\*,||,‡</sup>

<sup>†</sup>Department Pharmacology and Toxicology, <sup>‡</sup>Department of Anesthesia, and <sup>§</sup>Program in Medical Neuroscience, Paul and Carole Stark Neurosciences Research Institute, Indiana University School of Medicine, Indianapolis, Indiana 46202, United States

<sup>||</sup>Department of Chemistry and <sup>‡</sup>Division of Medicinal Chemistry and Natural Products, UNC Eshelman School of Pharmacy, University of North Carolina, Chapel Hill, North Carolina 27599, United States

**ABSTRACT:** We recently reported that merging key structural pharmacophores of the anticonvulsant drugs lacosamide (a functionalized amino acid) with safinamide (an  $\alpha$ -aminoamide) resulted in novel compounds with anticonvulsant activities superior to that of either drug alone. Here, we examined the effects of six such chimeric compounds on Na<sup>+</sup>-channel function in central nervous system catecholaminergic (CAD) cells. Using whole-cell patch clamp electrophysiology, we demonstrated that these compounds affected Na<sup>+</sup> channel fast and slow inactivation processes. Detailed electrophysiological characterization of two of these chimeric compounds that contained either an oxymethylene ((*R*)-7) or a chemical bond ((*R*)-11) between the two aromatic rings showed comparable effects on slow inactivation, use-dependence of block, development of slow inactivation, and recovery of Na<sup>+</sup> channels from inactivation. Both compounds were equally effective at inducing slow inactivation; (*R*)-7 shifted the fast inactivation curve in the hyperpolarizing direction greater than (*R*)-11, suggesting that in the presence of (*R*)-7 a larger fraction of the channels are in an inactivated state. None of the chimeric compounds affected veratridine- or KCl-induced glutamate release in neonatal cortical neurons. There was modest inhibition of KCl-induced calcium influx in cortical neurons. Finally, a single intraperitoneal administration of (*R*)-7, but not (*R*)-11, completely reversed mechanical hypersensitivity in a tibial-nerve injury model of neuropathic pain. The strong effects of (*R*)-7 on slow and fast inactivation of Na<sup>+</sup> channels may contribute to its efficacy and provide a promising novel therapy for neuropathic pain, in addition to its antiepileptic potential.

**KEYWORDS:** Lacosamide, safinamide, sodium channel, slow/fast inactivation, state-dependent, neuropathic pain



Recently, we reported a novel series of neurological compounds<sup>1</sup> that merged key pharmacophores found in two classes of clinical neurological agents, functionalized amino acids (FAAs, **2**)<sup>2–10</sup> and  $\alpha$ -amino acid amides (AAAs, **3**),<sup>11–15</sup> into the concise structure **1** (Figure 1). Lacosamide<sup>10</sup> (Vimpat, (*R*)-4) is the prototypical FAA and is a first-in-class antiepileptic drug (AED) that is marketed in the United States and Europe for adjunctive treatment of partial onset seizures in adults.<sup>16</sup> Safinamide ((*S*)-5) and ralfinamide ((*S*)-6) are representative AAAs, and both have undergone extensive clinical trials.<sup>11–15</sup> While (*S*)-5<sup>12,13</sup> and (*S*)-6<sup>14,15</sup> are potent anticonvulsants, Merck-Sorono has advanced (*S*)-5 for the treatment of Parkinson's disorders, and Newron has evaluated (*S*)-6 for neuropathic lower back pain. Recent, late-stage human clinical trials have indicated

that neither (*S*)-5 nor (*S*)-6 met their clinical end points, although they exhibited no undesirable side effects.<sup>17,18</sup>

At first glance, **2** and **3** appear similar in structure due to the vicinal diamine backbone that contains a carbonyl (C=O) moiety, the presence of one chiral center, and the inclusion of a *N*-benzyl (PhCH<sub>2</sub>)-type substituent. Pharmacologically, (*R*)-4, (*S*)-5, and (*S*)-6 exhibited excellent seizure protection<sup>10,19,20</sup> in the maximal electroshock seizure (MES) animal model,<sup>21</sup> and electrophysiology studies demonstrated that these agents modulated sodium currents.<sup>13,15,22,23</sup> However, (*R*)-4 selectively

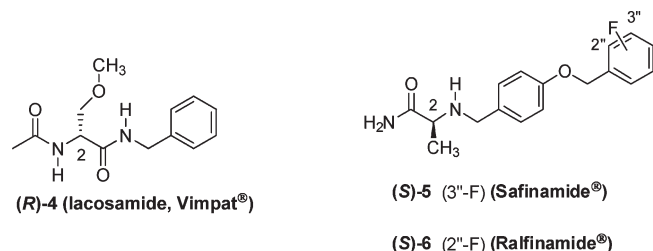
**Received:** March 11, 2011

**Accepted:** April 11, 2011

**Published:** April 11, 2011

enhanced the slow-inactivation state of the voltage-gated sodium channel (VGSC),<sup>22,23</sup> while (*S*)-5 inhibited tetrodotoxin-sensitive (TTX-S) fast sodium currents,<sup>13,24</sup> and (*S*)-6 modulated both sodium channel fast and slow inactivation processes.<sup>15</sup> The structural differences in (*R*)-4, (*S*)-5, and (*S*)-6 account for their different modes of action and underscore that each compound has distinctive pharmacophores that contribute to drug function.

We demonstrated that several **1s** displayed anticonvulsant activity in the MES seizure model that exceeded (*R*)-4, (*S*)-5, and established AEDs,<sup>25</sup> and exhibited pronounced activities in neuropathic pain animal models.<sup>1</sup> In this study, we evaluated selected **1s** by whole-cell, patch-clamp electrophysiology in catecholamine A differentiated (CAD) cells<sup>26,27</sup> and report their receptor binding profiles against a broad panel of neurological receptors. We find that while **1**, like (*R*)-4,<sup>27</sup> enhanced entry into the sodium channel slow-inactivation state, they were far more potent than (*R*)-4 in facilitating this transformation. Moreover, we show that, by varying the structure in **1**, sodium channel slow- and fast-inactivation processes can be modulated. When the **1s** were evaluated against a panel of 44 receptors known to impact drug effectiveness, we observed no significant binding. Similarly, the **1s** did not affect hERG K<sup>+</sup> channel activity. The potential neuropathic pain properties of two chimeric **1** agents were evaluated in a rat tibial-nerve injury (TNI) model.<sup>28</sup> Collectively, our pharmacological data indicate that **1s** exhibit a distinctive blend of pharmacological activities, providing compounds of neurological significance.



## RESULTS AND DISCUSSION

Structurally, **1s** can be viewed as consisting of three components (Figure 1, sectors A–C in **1**). The first is the *N*-acetyl amino acid *N'*-benzyl amide unit (sector A) seen in **2**. The second is the linker (X–Y–Z, sector B) that connects the two aryl groups. This moiety is present in **2**<sup>29</sup> and **3**. The final group is the terminal aromatic ring (sector C) seen in **3**. In our **1** structure–activity relationship (SAR) study, we varied one of these three components while retaining the same structural features seen in either (*R*)-4 or (*S*)-5 for the other two groups.<sup>1</sup> The anti-convulsant activities for the compounds were determined in the MES and the subcutaneous Metrazol<sup>30</sup> (scMet) tests at the National Institute of Neurological Disorders and Stroke (NINDS) Anticonvulsant Screening Program (ASP). Several structural principles emerged from this study. First, in sector A, successive increases in the size of the R group led to decreased anticonvulsant activity in the MES test. Second, including a substituted heteroatom one atom removed from the C(2) chiral center led to increased activity. Third, the observed anticonvulsant activity for **1** in the MES test principally resided in the D-configuration ((*R*)-stereoisomer). These three structural patterns were similar to those discovered for **2**.<sup>2–10</sup> Sector B consisted of the linker X–Y–Z unit. X–Y–Z is a molecular unit 1–3 atoms long, or it could also be a single bond. In sector B,

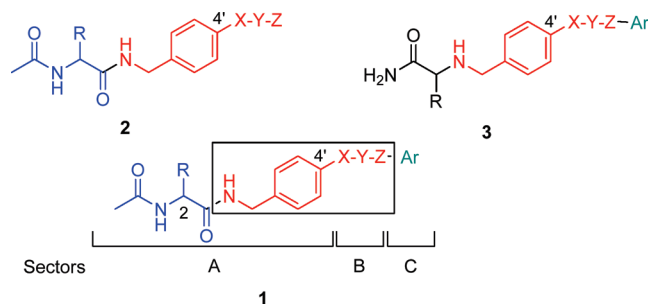


**Figure 1.** Overlay of pharmacophores in **1**. Structures of functionalized amino acids (**2**),  $\alpha$ -aminoamides (**3**), and chimeric agents **1**. The area of overlap in **1** (shown in box) permitted incorporating key pharmacophores found in **2** and **3** into a unified structure.

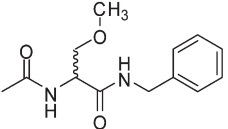
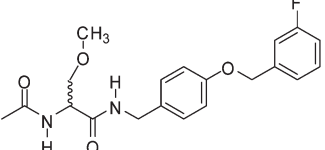
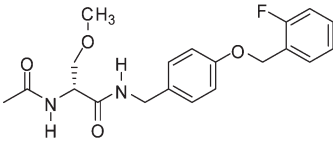
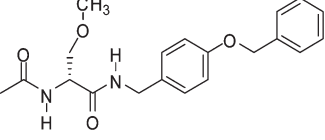
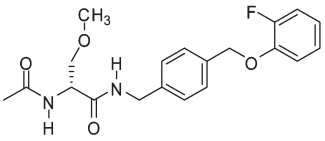
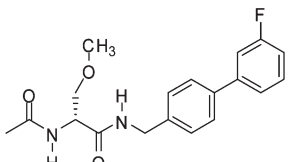
we found that the most potent **1** derivatives in the MES test were those in which X–Y–Z was a single bond, a rigid, linear (alkyne) unit, or a short moiety (O; X–Y, where X and Y are C(H), N(H), O, and CH<sub>2</sub>). For sector C, we found that the anti-convulsant activity could be altered several-fold by the substituent pattern in the terminal aryl (Ar) group. Both **1s**' chiral preference for the (*R*)-stereoisomer for blockage of MES-induced seizures and the absence of scMet seizure protection are hallmarks of FAA activity.<sup>2–10</sup> By comparison, (*S*)-5 and its stereoisomer (*R*)-5 have nearly equivalent activities in the MES test,<sup>11,31</sup> and (*S*)-5,<sup>32</sup> unlike **1**,<sup>1</sup> (*R*)-4,<sup>10</sup> or **2**,<sup>2–9</sup> displayed notable activity in the scMet model.

**Compound Selection.** Six **1s** (Table 1, compounds (*R*)-7, (*S*)-7, (*R*)-8, (*R*)-9, (*R*)-10, (*R*)-11) were examined by whole-cell, patch-clamp electrophysiology in CAD cells. For sector A in **1**, we selected the (*R*)-*N*-benzyl 2-acetamido-3-methoxypropionamide motif seen in (*R*)-4 since this unit exhibited the best activity in our SAR investigation.<sup>1</sup> Three units were chosen for sector B. They were the oxymethylene (OCH<sub>2</sub>) unit seen in both (*S*)-5 and (*S*)-6, the isomeric methyleneoxy (CH<sub>2</sub>O) unit, and the unit in which the ether linkages were deleted to give a chemical bond. For the terminal aryl unit, we selected compounds that were fluorinated at the 2'' (similar to (*S*)-6) or the 3'' (similar to (*S*)-5) position or was unsubstituted. Finally, we prepared the (*R*)- and (*S*)-enantiomers for a **1** derivative to provide information on the role of stereochemistry in cellular and receptor binding pharmacology. Significantly, (*R*)-7, (*R*)-8, (*R*)-9, (*R*)-10, and (*R*)-11 all exhibited excellent anticonvulsant activities in the MES seizure model<sup>21</sup> in rodents (ip, po), activities comparable to (*R*)-4 and that exceeded other antiepileptic drugs (Table 1).

**Chemistry.** Syntheses of (*R*)-7, (*S*)-7, (*R*)-8, (*R*)-9, and (*R*)-11 were previously reported.<sup>1</sup> We prepared (*R*)-10 using a method similar to the one for its isomer (*R*)-9 and using amine **15** and (*R*)-16 (Scheme 1). All compounds were fully characterized, and the enantiopurity of (*R*)-10 was assessed by detection of a single acetyl methyl and *O*-methyl signal in the <sup>1</sup>H NMR spectrum upon addition of a saturated solution of (*R*)-(-)-mandelic acid.<sup>33</sup>

**Receptor-Binding Profiles of Compounds **1s** on Human or Rodent Brain Receptors.** Primary radioligand binding profiles at UNC's National Institute of Mental Health (NIMH)-funded Psychoactive Drug Screening Program for **1** compounds were compared against a panel of 44 receptors and ion channels, including serotonin, adrenergic, dopamine, GABA, histamine, muscarinic, opioid, sigma, and transporters, and we saw no

Table 1. Anticonvulsant and Electrophysiology Data for 1 Agents

| Cpd No.   | Whole Animal Behavioral Studies    |                                    |                                    |                                    | IC <sub>50</sub> <sup>f</sup> value (μM) |
|---|------------------------------------|------------------------------------|------------------------------------|------------------------------------|--|
|   | Mice (ip) <sup>a</sup>             |                                    | Rat (po) <sup>d</sup>              |                                    |  |
|   | MES, <sup>b</sup> ED <sub>50</sub> | Tox, <sup>c</sup> TD <sub>50</sub> | MES, <sup>b</sup> ED <sub>50</sub> | Tox, <sup>e</sup> TD <sub>50</sub> |  |
|  (R)-4 <sup>g</sup>    | 4.5 [0.5]<br>(3.7 – 5.5)           | 27 [0.25]<br>(26 – 28)             | 3.9 [0.5]<br>(2.6 – 6.2)           | >500 [0.5]                         | 85                                       |
| (S)-4 <sup>g</sup>  | >100, <300                         | >300                               | >30                                | >30                                | >1000                                    |
|  (R)-7 <sup>h</sup>    | 13 [0.25]<br>(11 – 16)             | 26 [0.5]<br>(21 – 34)              | 14 [0.5]<br>(6.1 – 27)             | >500 [0.5]                         | 1.7                                      |
| (S)-7 <sup>h</sup>  | >300                               | >300                               | ND <sup>i</sup>                    | ND                                 | >2400                                    |
|  (R)-8 <sup>h</sup>    | 6.7 [0.25]<br>(4.8 – 9.1)          | 37 [0.5]<br>(29 – 48)              | 11 [0.5]<br>(7.9 – 13)             | >500                               | 1.6                                      |
|  (R)-9 <sup>h</sup>    | 5.8 [0.25]<br>(4.4 – 7.2)          | 22 [0.25]<br>(19 – 25)             | 5.6 [0.25]<br>(4.2 – 6.4)          | >250 [1.0]                         | 1.6                                      |
|  (R)-10               | 9.7 [0.25]<br>(7.9 – 12)           | 63 [0.25]<br>(48 – 81)             | ND                                 | ND                                 | 5.4                                      |
|  (R)-11 <sup>h</sup> | 12 [1]<br>(9.1 – 15)               | 50 [0.5]<br>(32 – 64)              | 2.4 [1.0]<br>(1.0 – 3.9)           | >500 [0.5]                         | 2.9                                      |
| Phenytoin <sup>j</sup>  | 9.5 [2.0]<br>(8.1 – 10)            | 66 [2.0]<br>(53 – 72)              | 30 [4.0]<br>(22 – 39)              | <i>k</i>                           | NS <sup>l,m</sup>                        |
| Phenobarbital <sup>j</sup>  | 22 [1.0]<br>(15 – 23)              | 69 [0.5]<br>(63 – 73)              | 9.1 [5.0]<br>(7.6 – 12)            | 61 [0.5]<br>(44 – 96)              | NS <sup>i</sup>                          |
| Valproate <sup>j</sup>  | 270 [0.25]<br>(250 – 340)          | 430 [0.25]<br>(370 – 450)          | 490 [0.5]<br>(350 – 730)           | 280 [0.5]<br>(190 – 350)           | NS <sup>i</sup>                          |

<sup>a</sup>The compounds were administered intraperitoneally. ED<sub>50</sub> and TD<sub>50</sub> values are in milligrams per kilogram. Numbers in parentheses are 95% confidence intervals. The dose effect was obtained at the time of peak effect (indicated in hours in brackets). <sup>b</sup>MES = maximal electroshock seizure test. <sup>c</sup>TD<sub>50</sub> value determined from the rotarod test. <sup>d</sup>The compounds were administered orally. ED<sub>50</sub> and TD<sub>50</sub> values are in milligrams per kilogram. <sup>e</sup>Tox = behavioral toxicity. <sup>f</sup>IC<sub>50</sub>. Concentration at which half of the Na<sup>+</sup> channels have transitioned to a slow inactivated state. <sup>g</sup>Reference 10. <sup>h</sup>Reference 1. <sup>i</sup>ND = not determined. <sup>j</sup>Reference 25. <sup>k</sup>No ataxia observed up to 3000 mg/kg. <sup>l</sup>NS, not selective for slow inactivation. <sup>m</sup>References 22 and 56.

significant binding at 10 μM of compounds (data not shown). When the six 1 compounds (10 μM) were evaluated in the hERG K<sup>+</sup> channel assay using a fluorescence-based membrane potential assay, no activity was observed (data not shown). Three of the six (9, 10, 11) exhibited modest binding (~31–46% displacement at 10 μM) for site 2 sodium channel binding when tested at Cerep (data not shown).

**Robust Inhibition of Na<sup>+</sup> Currents by 1 Agents.** Using the whole-cell patch-clamp configuration, we examined the effects of the six chimeric compounds on voltage-gated Na<sup>+</sup> channels in

CAD cells. We have previously shown that CAD cells express endogenous tetrodotoxin-sensitive Na<sup>+</sup> currents with rapid activation and inactivation upon membrane depolarization and are likely composed of Na<sub>v</sub>1.7, Na<sub>v</sub>1.1, and Na<sub>v</sub>1.3 channels.<sup>27</sup> We also showed that (R)-4 inhibited peak Na<sup>+</sup> currents by ~40%, while the inactive enantiomer (S)-4 exhibited no inhibition. Here, the ability of 1 agents to inhibit peak inward Na<sup>+</sup> currents was tested by holding CAD cells at –80 mV and running a current (*I*)–voltage (*V*) protocol, which consisted of 15 ms step depolarizations ranging from –70 to +80 mV (in +10 mV

## Scheme 1. Synthesis of (R)-10

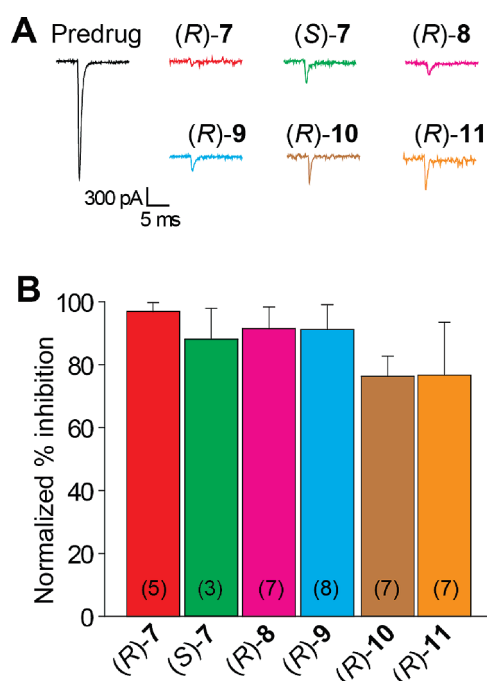
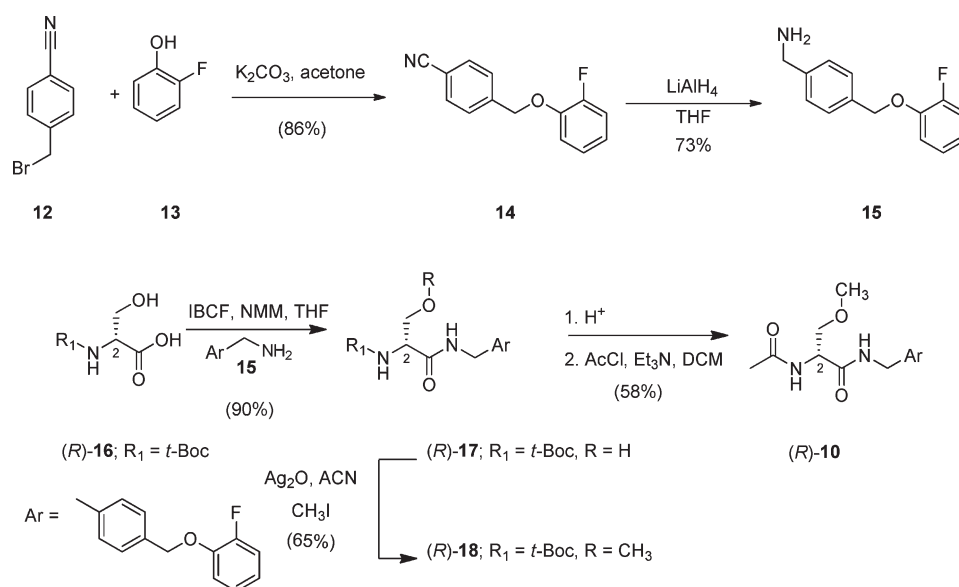


**Figure 2.** Inhibition of Na<sup>+</sup> currents by chimeric **1** derivatives. (A) Representative peak Na<sup>+</sup> current responses, evoked by a step from a holding potential of  $-80$  to  $0$  mV, of CAD cells treated with 0.1% DMSO control (predrug),  $30 \mu\text{M}$  (R)-7,  $500 \mu\text{M}$  (S)-7,  $100 \mu\text{M}$  (R)-8, (R)-9, or (R)-10, or  $30 \mu\text{M}$  (R)-11. These currents illustrate the maximal inhibition achievable at the highest concentrations used for each **1**. (B) Percent inhibition of peak current density (pA/pF) for the indicated **1**s measured at  $0$  mV in CAD cells. Inhibition was determined by normalizing peak currents in each drug condition to average peak currents obtained in DMSO-treated cells. Numbers in parentheses are the number of cells patched per condition. IC<sub>50</sub> values of the peak Na<sup>+</sup> currents are presented in Table 2.

increments). Figure 2A shows representative peak Na<sup>+</sup> currents, elicited by a step to  $0$  mV, recorded from CAD cells treated with

**Table 2.** Effects of **1** agents on inhibition of peak Na<sup>+</sup> current

| compd  | peak inhibition IC <sub>50</sub> (μM) <sup>a</sup> |
|--------|--|
| (R)-4  | 132.6 ± 9.8  |
| (S)-4  | >500   |
| (R)-7  | 13.6 ± 4.1   |
| (S)-7  | 42.9 ± 1.4   |
| (R)-8  | 1.1 ± 0.4  |
| (R)-9  | 7.3 ± 2.0  |
| (R)-10 | 4.9 ± 0.9  |
| (R)-11 | 2.2 ± 0.9  |

<sup>a</sup>IC<sub>50</sub> values were calculated by regression analysis from at least five different concentrations.

0.1% dimethyl sulfoxide (DMSO; predrug control) or highest concentrations used for each of the **1** agents. All chimeric compounds greatly inhibited peak Na<sup>+</sup> currents at concentrations of  $30 \mu\text{M}$  and higher (Figure 2B). These peaks were normalized by cell capacitance and were expressed as peak current density (pA/pF) to account for variations in cell size. Dose–response curves for percent inhibition of peak Na<sup>+</sup> currents were constructed and yielded IC<sub>50</sub> values, that is, a concentration at which half of the peak Na<sup>+</sup> current is inhibited (Table 2). These results show that the **1** agents are far better inhibitors of peak Na<sup>+</sup> currents than (R)-4. Na<sup>+</sup> current inhibition was not accompanied by changes in reversal potential, half-maximal activation, or slope parameters (see Figure 4) for any of the chimeric derivatives.

**1** Agents Affect the Transition to a Slow-Inactivated State of Na<sup>+</sup> Currents in CAD Cells. Consistent with earlier observations,<sup>22,23</sup> we recently reported that (R)-4 reduces VGSC availability by selectively enhancing the transition to a slow-inactivated state of VGSCs.<sup>27,34</sup> Therefore, we tested the ability of chimeric **1** to modulate transition to a slow-inactivated state in CAD cells. CAD cells were held at  $-80$  mV and conditioned to potentials ranging from  $-120$  to  $+20$  mV (in  $+10$  mV increments) for  $5$  s. Then, fast-inactivated channels were allowed

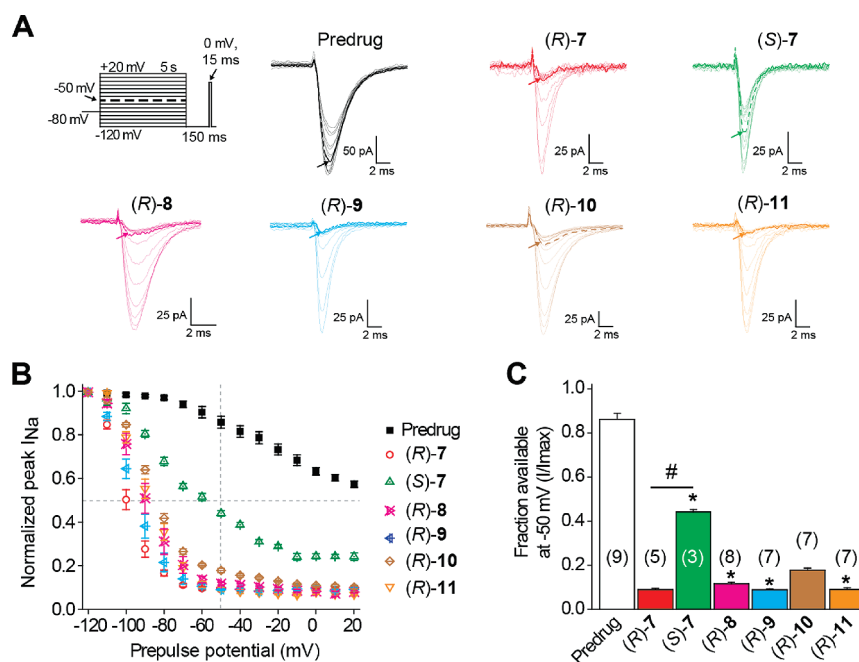


**Figure 3.** **1s** affect steady-state slow-inactivation state of  $\text{Na}^+$  currents in CAD cells. (A) Currents were evoked by 5 s prepulses between  $-120$  and  $-20$  mV and then fast-inactivated channels were allowed to recover for 150 ms at a hyperpolarized pulse to  $-120$  mV. The fraction of channels available at 0 mV was analyzed. Representative current traces from CAD cells in the absence (predrug, 0.1% DMSO) or presence of **1s**, as indicated. Illustrated currents are from concentrations of **1s** described in the legend to Figure 2. The dashed traces in each panel represent the current at  $-50$  mV (also highlighted in the voltage protocol). (B) Summary of steady-state, slow-activation curves for CAD cells treated with DMSO (predrug) or **1** compounds. Drug-induced slow inactivation was prominent in CAD cells treated with all **1s** except (*S*)-**7**, which influenced slow inactivation to a lesser extent than the (*R*)-enantiomers. (C) Summary of the fraction of current available at  $-50$  mV for CAD cells in the absence or presence of (*R*)- or (*S*)-enantiomers of the indicated compounds. Asterisks (\*) indicate statistically significant differences in fraction of current available between predrug and (*R*)- and (*S*)- compounds ( $p < 0.05$ , Student's *t*-test). Hash mark (#) indicates a statistically significant difference in fraction of current available between (*R*)- and (*S*)-enantiomers of **7**. Data are from 3–9 cells per condition, as indicated. The half-maximal values for slow inactivation for all compounds are shown in Table 1.

to recover for 150 ms at a hyperpolarized pulse to  $-120$  mV, and the fraction of channels available was tested by a single depolarizing pulse, to 0 mV, for 15 ms (Figure 3A, top left). This brief hyperpolarization allowed the channels to recover from fast inactivation while limiting recovery from slow inactivation.

A representative family of slow-inactivation traces from CAD cells treated with 0.1% DMSO (predrug) or various concentrations of (*R*)-**7**, (*S*)-**7**, and (*R*)-**8**–(*R*)-**11** are shown in Figure 3A. For comparison, representative current traces at  $-50$  mV are highlighted. This potential was chosen for three reasons: (1) a large fraction of channels are undergoing steady-state inactivation, which involves contributions from slow- and fast-inactivating pathways<sup>35,36</sup> where  $-50$  mV is within the steep voltage-dependence range for each, (2) it is near the resting membrane potential (RMP) and approaches the action potential firing threshold for CNS neurons,<sup>37</sup> where slow inactivation appears to be physiologically relevant during sustained subthreshold depolarizations,<sup>38</sup> and (3) changes in the  $\text{Na}^+$  channel availability near  $-50$  mV can impact the overlap of  $\text{Na}^+$  current activating and inactivating under steady-state conditions.<sup>36,39</sup> Adding  $30 \mu\text{M}$  (*R*)-**7** to CAD cells significantly decreased the fraction of current available, compared with cells without drug. (*S*)-**7**, at the highest dose of  $500 \mu\text{M}$ , reduced the available current but not to the extent observed with (*R*)-**7**. At  $-50$  mV,  $0.91 \pm 0.01$  fractional units ( $n = 5$ ) of the  $\text{Na}^+$  current were available in DMSO-treated cells, suggesting a large fraction ( $0.09 \pm 0.01$ ; calculated as 1 minus the normalized  $I_{\text{Na}}$ ) of the channels transitioned to a nonconducting (slow-inactivated)

state in (*R*)-**1**-treated cells (Figure 3B, C). These findings are consistent with earlier results that showed that (*R*)-**4** promoted slow inactivation in recombinant h $\text{Na}_v1.7$  channels expressed in HEK cells.<sup>23</sup> The similarity of our data to these earlier findings support our use of CAD cells to elucidate the effects of the chimeric derivatives on  $\text{Na}^+$  channel function.

Using this patch-clamp protocol, slow inactivation was observed at potentials more depolarized than  $-100$  mV for (*R*)-**7**–(*R*)-**11** with the exception of (*S*)-**7**, for which it was observed at potentials more depolarized than  $-80$  mV (Figure 3B). Each of the chimeric **1** agents caused a significant increase in the maximal fraction of current unavailable by depolarization (20 mV; control,  $0.42 \pm 0.02$ ,  $n = 98$ ;  $30 \mu\text{M}$  (*R*)-**7**,  $0.91 \pm 0.01$ ,  $n = 5$ ;  $500 \mu\text{M}$  (*S*)-**7**,  $0.76 \pm 0.02$ ,  $n = 3$ ;  $100 \mu\text{M}$  (*R*)-**8**,  $0.93 \pm 0.005$ ,  $n = 8$ ;  $100 \mu\text{M}$  (*R*)-**9**,  $0.92 \pm 0.008$ ,  $n = 7$ ;  $100 \mu\text{M}$  (*R*)-**10**,  $0.90 \pm 0.007$ ,  $n = 7$ ; and  $30 \mu\text{M}$  (*R*)-**11**,  $0.94 \pm 0.004$ ,  $n = 7$ ;  $p < 0.01$ , Mann–Whitney U test).

To further understand the extent to which the hybrid **1** agents induce slow inactivation, we performed concentration response curves for slow-inactivation induction for each compound. Using the Boltzmann equation, we fit the voltage-dependence of slow-inactivation for control and each of the drug concentrations. This yielded a  $V_{1/2}$  value of slow inactivation for each concentration which was then plotted against the concentration used. Finally, fits of the concentration–response of slow inactivation against the  $V_{1/2}$  of slow inactivation provided an  $\text{IC}_{50}$  value. Table 1 shows these values for slow inactivation induced by chimeric **1**

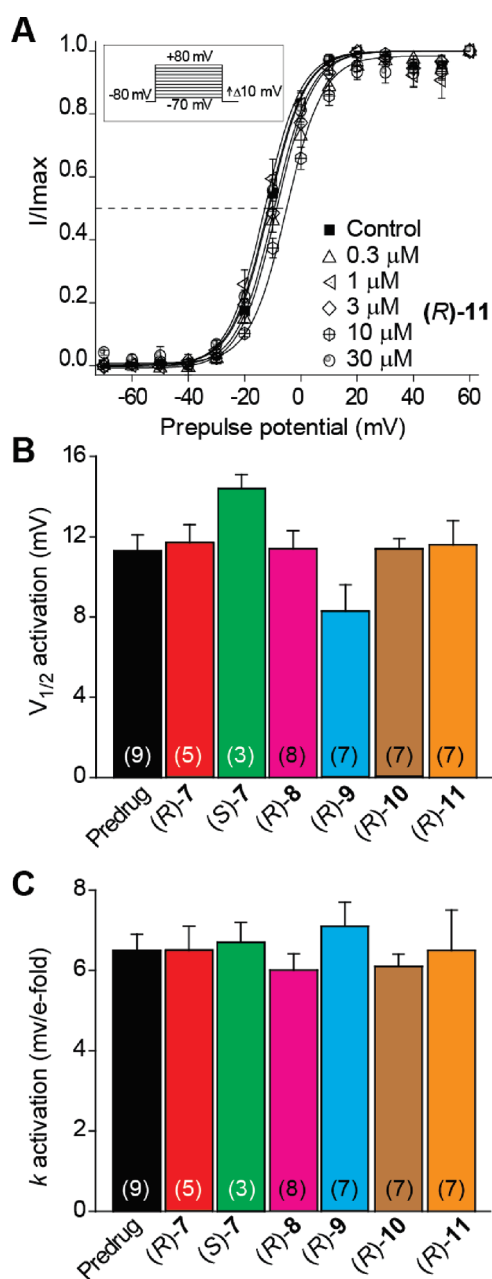


**Figure 4.** Activation properties of  $\text{Na}^+$  currents are not affected by 1 compounds in CAD cells. Values for the voltage of half-maximal activation ( $V_{1/2}$ ) and the slope factors ( $k$ ) were derived from Boltzmann distribution fits to the individual recordings and averaged to determine the mean ( $\pm$ SEM) voltage dependence of activation. The voltage protocol used to evoke current responses is shown in the inset in (A). Representative Boltzmann fits for 0.03% DMSO (control) and 0.3–30  $\mu\text{M}$  (R)-11 are shown (A). The  $V_{1/2}$  (B) and  $k$  (C) of activation were not different among the 1 compounds tested ( $p > 0.05$ , one-way ANOVA). Data are from 3–9 cells per condition.

compounds. Compared with our recently reported  $\text{IC}_{50}$  calculated value of 85  $\mu\text{M}$  for slow inactivation induced by (R)-4,<sup>27</sup> the  $\text{IC}_{50}$  value for the 1 agents was 16- (for (R)-10) to 53-fold (for (R)-8 and (R)-9) lower.

Collectively, these data indicate that the chimeric agents (R)-7–(R)-11 are more effective at inducing the transition of  $\text{Na}^+$  channels to a slow-inactivated state than is (R)-4.

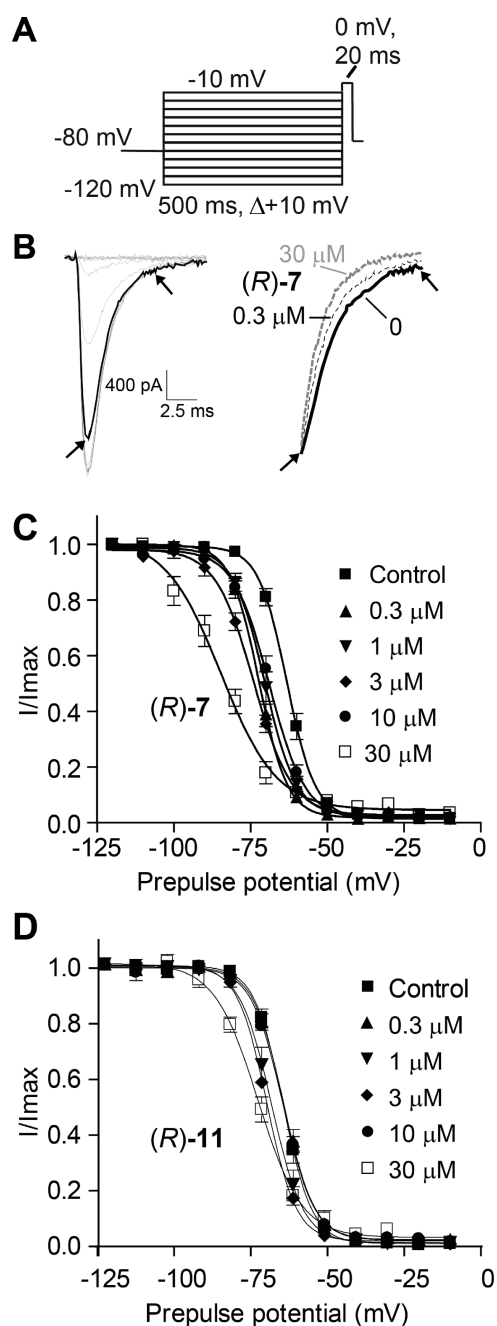


**Figure 5.** Fast inactivation properties of  $\text{Na}^+$  currents are affected by 1 compounds in CAD cells. (A) Voltage protocol for fast inactivation. (B) Representative current traces showing voltage-dependent fast inactivation of  $\text{Na}^+$  currents from CAD cells treated with 0.03% DMSO control (left). Right: An enlarged region of the inactivating portion of current traces (from a step to  $-70$  mV) between the arrows from a CAD cell without drug (0, thick black trace), with 0.3  $\mu\text{M}$  (R)-7 (thin broken black line), or with 30  $\mu\text{M}$  (R)-7 (thick dotted gray line). Note the faster inactivation in the presence of (R)-7. (C) Representative Boltzmann fits for 0.03% DMSO (control) and 0.3–30  $\mu\text{M}$  (R)-7. Values for the voltage of half-maximal inactivation ( $V_{1/2}$ ) and the slope factors ( $k$ ) were derived from Boltzmann distribution fits to the individual recordings and averaged to determine the mean ( $\pm$ SEM) voltage dependence of steady-state inactivation. (D) Adding increasing concentrations of (R)-11 led to a hyperpolarizing shift in the  $V_{1/2}$  of fast inactivation. The  $k$  values of steady-state fast inactivation were not different among the conditions tested ( $p > 0.05$ , one-way ANOVA).

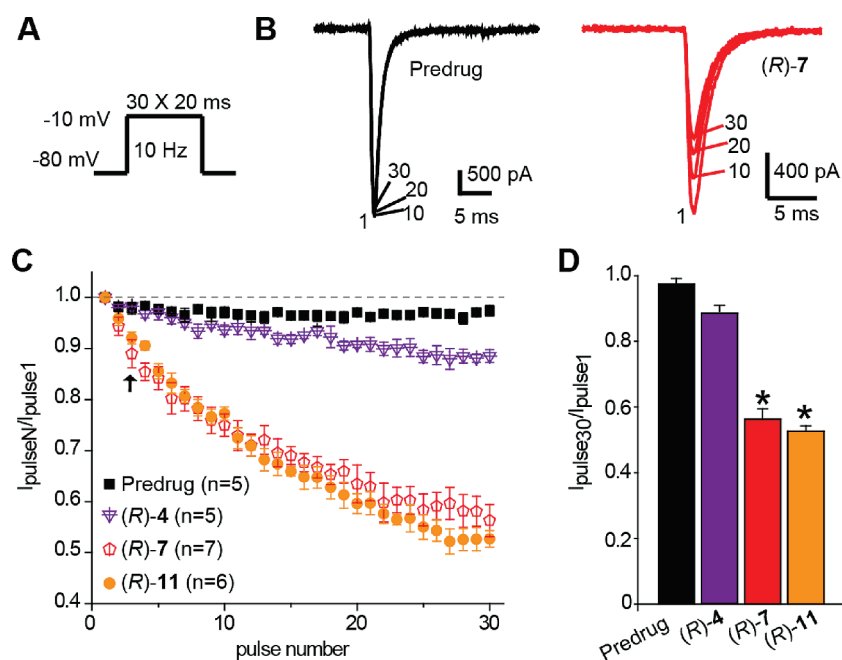


**Figure 6.** Significant frequency-dependent block by (R)-7 and (R)-11 of  $\text{Na}^+$  currents in CAD cells. (A) The frequency dependence of block was examined by holding cells at the hyperpolarized potential of  $-80$  mV and evoking currents at  $10$  Hz by  $20$  ms test pulses to  $-10$  mV. (B) Representative overlaid traces are illustrated by pulses 1, 10, 20, and 30 for control (predrug) and in the presence of (R)-7 ( $8.5 \mu\text{M}$ ) and (R)-11 ( $15 \mu\text{M}$ ). For clarity, the use dependence traces for (R)-4 and (R)-11 are not shown. (C) Summary of average frequency-dependent decrease in current amplitude ( $\pm$ SEM) produced by (R)-4 ( $100 \mu\text{M}$ ), (R)-7, and (R)-11 but not by control conditions. (D) Summary of the maximal decrement in current amplitude observed at the end of the 30 pulse train for predrug, (R)-4, (R)-7, and (R)-11. (R)-7 and (R)-11 show a significant decrease in current amplitude compared with pretreatment ( $*$ ,  $p < 0.05$ , one-way ANOVA with Dunnett's posthoc test). Note the rapid frequency-dependent facilitation of block by both (R)-7 and (R)-11 that was observed beginning as early as pulse 3 (arrow). Data are from 5–7 cells per condition.

**Activation Properties of  $\text{Na}^+$  Currents in CAD Cells Are Not Affected by the 1 Agents.** Because changes in current amplitudes can result from changes in channel gating,<sup>40</sup> we tested whether the 1 agents could alter voltage-dependent activation properties of  $\text{Na}^+$  currents in CAD cells. Changes in activation for the CAD cells treated with the derivatives were measured by whole-cell ionic conductances by comparing their midpoints ( $V_{1/2}$ ) and slope factors ( $k$ ) in response to changes in command voltage (Figure 4A, inset). Representative Boltzmann fits for DMSO (predrug) and  $0.3$ – $30 \mu\text{M}$  (R)-11 are shown in Figure 4A. An analysis of (R)-7–(R)-11 (only highest concentrations illustrated)  $V_{1/2}$  (Figure 4B) and  $k$  (Figure 4C) values showed that there were no changes in the steady-state activation properties of  $\text{Na}^+$  currents between CAD cells treated with DMSO control or with any of the tested compounds. These data indicate that chimeric 1 derivatives do not affect the channel's transition from a closed to an open conformation.

**Fast Inactivation Properties of  $\text{Na}^+$  Currents in CAD Cells Are Affected by 1 Agents.** Our data indicated that hybrid agents (R)-7–(R)-11 exhibit profound effects on the slow inactivated state of  $\text{Na}^+$  channels. We next asked if these agents could enhance steady-state fast inactivation. To find out, we used a protocol (Figure 5A) designed to induce a fast-inactivated state, as previously described.<sup>27</sup> Cells were held at  $-80$  mV, stepped to inactivating prepulse potentials ranging from  $-120$  to  $-10$  mV (in  $10$  mV increments) for  $500$  ms, and then the cells were stepped to  $0$  mV for  $20$  ms to measure the available current. A  $500$  ms conditioning pulse was used because it allowed all of the endogenous channels to transition to a fast-inactivated state at all potentials assayed. Steady-state, fast inactivation curves of  $\text{Na}^+$

currents from DMSO- and all (R)-7–(R)-11–treated CAD cells were well fitted with a single Boltzmann function ( $R^2 > 0.9942$  for all conditions). The  $V_{1/2}$  value for inactivation for  $0.1\%$  DMSO-treated cells was  $-63.2 \pm 0.9$  mV ( $n = 8$ ), which was significantly different from that of (R)-7 ( $30 \mu\text{M}$ )-treated cells ( $-84.6 \pm 1.2$  mV;  $n = 8$ ;  $p < 0.05$ ; Student's  $t$ -test; see Figure 5C). Compared with the  $\sim 21.4$  mV shift in  $V_{1/2}$  of fast inactivation in the hyperpolarizing direction observed in the presence of (R)-7, the shifts caused by the other 1 agents were as follows:  $19.9$  mV, (S)-7 ( $500 \mu\text{M}$ ;  $n = 7$ );  $16.8$  mV, (R)-8 ( $100 \mu\text{M}$ ;  $n = 7$ );  $21.7$  mV, (R)-9 ( $100 \mu\text{M}$ ;  $n = 7$ );  $17.6$  mV, (R)-10 ( $100 \mu\text{M}$ ;  $n = 7$ ); and  $8.0$  mV, (R)-11 ( $30 \mu\text{M}$ ;  $n = 7$ ; Figure 5D) ( $p < 0.05$  vs DMSO control; Student's  $t$ -test). By comparison, we observed a  $0.7$  mV shift with (R)-4 ( $30 \mu\text{M}$ ).<sup>27</sup> Additionally, the time constant for inactivation ( $\tau_{\text{inact}}$ ) was faster with (R)-7, compared with DMSO:  $0.73 \pm 0.05$  ms for  $0.3 \mu\text{M}$  (R)-7 ( $n = 6$ ) versus  $1.32 \pm 0.12$  ms for DMSO ( $n = 6$ ; see Figure 5B, right).

**Frequency-Dependent Block of  $\text{Na}^+$  Currents by 1 Agents on CAD Cells.** We selected (R)-7 and (R)-11 to study the frequency-dependent block (and development of inhibition/slow inactivation; see next section) of  $\text{Na}^+$  currents. (R)-7 and (R)-11 have comparable structures except their linker units (Figure 1, sector B) between the two aromatic rings. In (R)-7, sector B is the oxymethylene unit ( $\text{OCH}_2$ ) found in (S)-5, and in (R)-11 it is a chemical bond. The ability to block  $\text{Na}^+$  currents in an activity- or use-dependent manner is a useful property for antiepileptic drugs, since it allows for preferential decreases in  $\text{Na}^+$  channel availability during high- (i.e., seizures) but not low-frequency firing. Thus, we tested if (R)-7 ( $8.5 \mu\text{M}$ ) and (R)-11 ( $15 \mu\text{M}$ ) could elicit use-dependent block. These concentrations

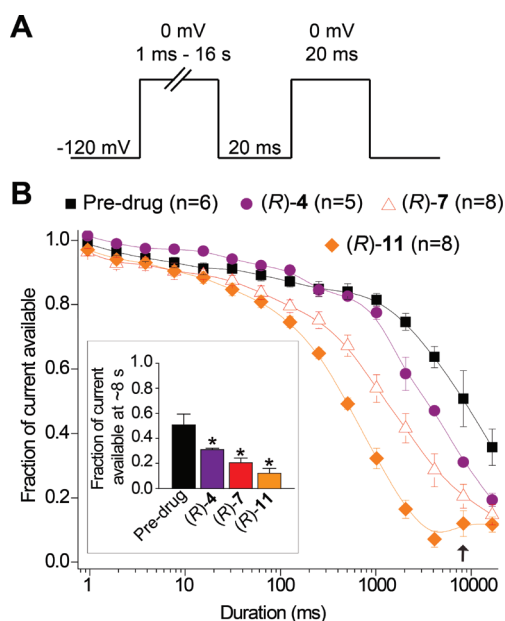


**Figure 7.** Inhibition/slow inactivation development rate is altered by (R)-7 and (R)-11 in CAD cells. (A) Voltage protocol for development of inhibition/slow inactivation. Following a variable conditioning pulse to 0 mV, a 20 ms pulse to  $-120$  mV allows recovery from fast inactivation (but not block) before the fraction of current available with the 20 ms pulse to 0 mV. (B) (R)-7 and (R)-11 increased the inactivation/inhibition development rate over that observed in vehicle-treated CAD cells at prepulse durations greater than 128 ms ( $p < 0.05$ , one-way ANOVA with Dunnett's posthoc test). Inset: the fraction of current available at 8 s (arrow) prepulse duration was significantly smaller for (R)-4 ( $0.32 \pm 0.01$ ,  $n = 5$ ), (R)-7 ( $0.20 \pm 0.04$ ,  $n = 8$ ), and (R)-11 ( $0.12 \pm 0.04$ ,  $n = 8$ ) than for vehicle-treated cells ( $0.52 \pm 0.09$ ,  $n = 6$ ;  $p < 0.05$ , one-way ANOVA with Dunnett's posthoc test).

were used because they are  $\sim 5$ -fold above the  $IC_{50}$  values for slow inactivation for these compounds. A train of 30 test pulses (20 ms to  $-10$  mV) was delivered from a holding potential of  $-80$  mV at 10 Hz (Figure 6A). The available current in control cells and cells in the presence of 1 agents was calculated by dividing the peak current at any given pulse (pulse<sub>N</sub>) by the peak current in response to the initial pulse (pulse<sub>1</sub>). Both (R)-7 and (R)-11 reduced current amplitude compared with control (Figure 6B–D). When we tested (R)-4 (100  $\mu$ M), we also observed a small level of block, consistent with our previous findings.<sup>27</sup> While use-dependent block by (R)-4 was first observed by about pulse 19 in the train, (R)-7 and (R)-11 did not show such latency, with rapid block seen as early as pulse 3 (Figure 6C, arrow). By the last pulse, compared with control, the peak current was  $\sim 9\%$  lower in the presence of (R)-4, 40% lower in the presence of (R)-7, and 45% lower in the presence of (R)-11 (Figure 6D).

**Inhibition/Slow Inactivation Development Rate Is Altered by (R)-7 and (R)-11 in CAD Cells.** To understand the interaction between (R)-7 and (R)-11 and  $Na^+$  channels, we next investigated the time course of block development by these agents and compared the results with (R)-4. Block development was examined by holding the cells at  $-120$  mV in the absence or presence of (R)-4 (100  $\mu$ M), (R)-7 (8.5  $\mu$ M), and (R)-11 (15  $\mu$ M), prepulsing the cells to 0 mV for varying amounts of time to allow block to develop, hyperpolarizing the cells to  $-120$  mV for 20 ms to allow unbound channels to recover from fast inactivation, and

then stepping the cells to 0 mV for 20 ms to determine the fraction of channels available for activation (Figure 7A). The reduction in the fraction of current available is indicative of the time course for the development of slow inactivation. The time course for reducing channel availability without drug as well as in the presence of (R)-7 and (R)-11 was biphasic, with a fast component likely representing block development of fast-inactivated channels and a slow component consistent with the time course of slow inactivation development (Figure 7B). The time constant for block development was  $\sim 2$ -, 4-, and 8-fold faster in cells treated with (R)-4 (100  $\mu$ M), (R)-7 (8.5  $\mu$ M), and (R)-11 (15  $\mu$ M), respectively, than that with vehicle-treated control cells. Both (R)-7 and (R)-11 caused reductions in the fraction of current at 8 s (Figure 7B, inset) compared with control cells ( $p < 0.05$ , one-way ANOVA with Dunnett's posthoc test).

**Inactivation/Block Recovery Is Altered by (R)-7 and (R)-11 in CAD Cells.** We also examined the rate at which  $Na^+$  channels in CAD cells recovered from inactivation and/or block by (R)-7 and (R)-11, and the results were compared with (R)-4. Cells ( $n = 5$ –7 for each condition) were held at  $-120$  mV, depolarized to 0 mV for 10 ms, and then hyperpolarized to  $-120$  mV for variable increasing durations before testing the available current with a step depolarization to 0 mV (Figure 8A). The time course of recovery from the 10 ms depolarization was not different from control for currents recorded in the presence of (R)-4 or (R)-11, although a slight slowing was observed in the presence of (R)-7 (Figure 8B). In another set of experiments, cells were held at  $-120$  mV, depolarized to 0 mV to 5 s, and then hyperpolarized to  $-120$  mV for a variable duration before testing the available current with a step depolarization to 0 mV (Figure 8C). The 5 s depolarization provides sufficient time for the channels to undergo slow inactivation. The time course for recovery from the 5 s depolarization was dramatically different from that of control cells for currents recorded in the presence of (R)-7 and (R)-11 (Figure 8D). The time constant for recovery from the 5 s prepulse was significantly greater in the presence of either (R)-7 or (R)-11 ( $p < 0.01$  at 100 ms to 2 s; Figure 8D) and lesser for (R)-4 (between 100 to 500 ms;  $p < 0.01$ ; Figure 8D).

**1 Agents Do Not Affect Veratridine- or Potassium Chloride (KCl)-Induced Glutamate Release from Cortical Neurons.** Since glutamate levels are higher in human epileptogenic foci<sup>41</sup> and inhibition of glutamate release by antiepileptics such as phenytoin, carbamazepine, and lamotrigine<sup>42</sup> has been reported, we examined whether inhibition of glutamate release might contribute to the anticonvulsant properties of any of the novel 1 agents in embryonic cortical neurons. As shown in Figure 9A, the initial basal or resting release of glutamate was not significantly different among any of the conditions. KCl (90 mM) evoked a significant increase in glutamate release under all conditions; however, there were no differences in the maximal glutamate released by KCl from cells treated with DMSO (control) or with any of the compounds tested (Figure 9A). The evoked glutamate release (stimulated minus initial basal release) was also not different for any of the conditions tested (Figure 9A). The total content of glutamate, measured at the end of the release experiment, was not different between the control and any of the drug conditions ( $p > 0.05$ , ANOVA with a Tukey's posthoc test; Figure 9B). We also found that veratridine, another membrane depolarizing agent that acts via activating sodium channels, did not affect evoked glutamate levels (Table 3). Notably, veratridine specifically modifies open sodium channels and requires depolarization for this modification to occur.<sup>43</sup>



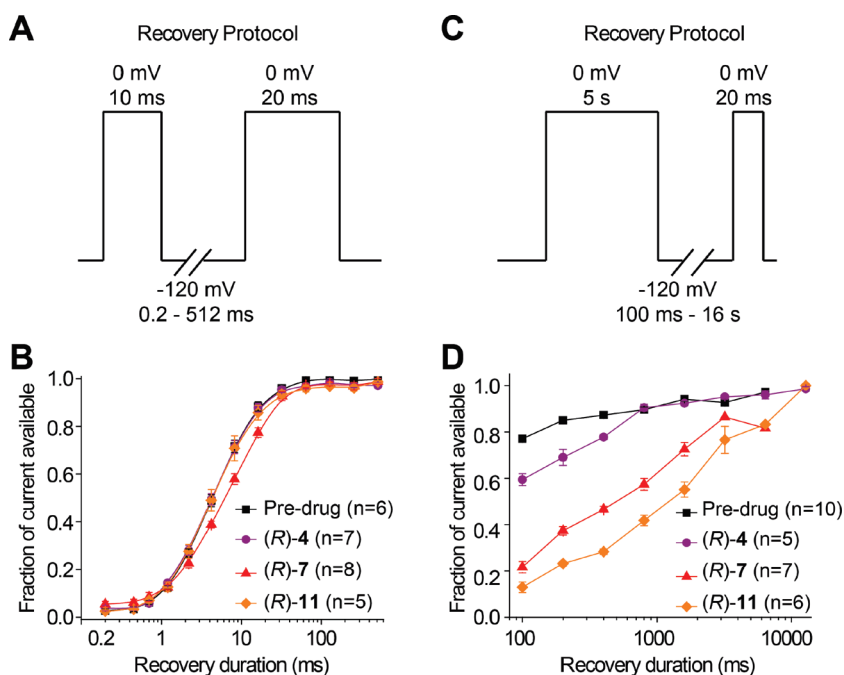


**Figure 8.** Effects of **1** compounds on  $\text{Na}^+$  channel inactivation recovery. (A,B) Voltage protocols for recovery of  $\text{Na}^+$  currents. CAD cells were held at  $-120$  mV, depolarized to 0 mV for 10 ms or 5 s, and then hyperpolarized to  $-120$  mV for varying increasing durations before testing the available current with a step depolarization to 0 mV. Data sweeps were acquired at 0.5 Hz for short recovery durations and at slower rates for the longer recovery durations. (C) (R)-7 ( $8.5 \mu\text{M}$ ) caused a small decrease in the rate of inactivation/inhibition recovery (10 ms prepulse) for  $\text{Na}^+$  channels, whereas (R)-4 and (R)-11 had no effect. (D) (R)-4 ( $100 \mu\text{M}$ ), (R)-7 and (R)-11 ( $15 \mu\text{M}$ ) slowed recovery kinetics after slow inactivation was induced, compared with control. In the presence of any of the three compounds, the fraction of available channels after a 5 s depolarization was lower for all three drugs than for control, and the duration of recovery was longer (significant between 100 ms and 2 s; except for (R)-4 where significance was observed between 100 and 512 ms) than that of the control. Numbers in parentheses indicate number of cells patched per condition.

Another reason why veratridine did not affect  $\text{Ca}^{2+}$  release here is that veratridine itself abolishes inactivation.<sup>44</sup> Since KCl-induced depolarization of glutamate release depends on  $\text{Ca}^{2+}$  influx via high threshold voltage-gated  $\text{Ca}^{2+}$  channels, these results suggest that **1** agents do not target these  $\text{Ca}^{2+}$  channels (see next section).

**1 Agents Induce Modest Inhibition of Calcium Influx in Cortical Neurons.** We next wanted to test if chimeric compounds **1** affected depolarization-induced  $\text{Ca}^{2+}$  influx in primary neurons. Changes in intracellular  $\text{Ca}^{2+}$  were measured in E18 rat cortical neurons using the ratiometric  $\text{Ca}^{2+}$ -sensitive dye Fura-2.  $\text{Ca}^{2+}$  release was evoked by successive pulses of KCl 5 min apart (Figure 10A). Exposing cells to (R)-4 ( $100 \mu\text{M}$ ) prior to the second KCl pulse resulted in a  $9.24 \pm 1.66\%$  inhibition of  $\text{Ca}^{2+}$  amplitude compared with  $13.74 \pm 1.26\%$  inhibition for (S)-4 (Figure 10B). These results are consistent with our recent electrophysiological study in which we found no effects of (R)-4 on  $\text{Ca}^{2+}$  currents via N- or P/Q-type voltage-gated calcium channels in hippocampal neurons.<sup>45</sup> All **1**s, except (S)-7, showed a modest but significant increase in percent inhibition compared with (R)-4 ( $p < 0.05$ , one-way ANOVA with Dunnett's posthoc test). Maximal inhibition of  $\text{Ca}^{2+}$  influx ( $17.3 \pm 1.5\%$ ) was observed with (R)-9 ( $100 \mu\text{M}$ ). However, this is relatively small compared with  $63.3 \pm 1.6\%$  inhibition ( $n = 84$ ) observed following incubation with Nifedipine ( $10 \mu\text{M}$ ), a well-established L-type  $\text{Ca}^{2+}$  channel inhibitor. These results suggest that **1**s have a modest effect on depolarization-induced  $\text{Ca}^{2+}$  influx.

**Neuropathic Pain is Reversed by Treatment With (R)-7 but Not (R)-11.** We next examined the effects of (R)-7 and (R)-11 on

established chronic nociceptive behavior in an animal model of TNI-mediated neuropathic pain.<sup>28</sup> TNI induces rapid onset and prolonged chronic behavioral hypersensitivity to mechanical and thermal stimuli.<sup>28</sup> Here, the ability of (R)-7 and (R)-11 to reverse tactile hypersensitivity was evaluated in rats at 14 and 28 days after TNI. Fourteen days following TNI, all animals exhibited pronounced mechanical allodynia ( $36.1 \pm 3.9$  mN;  $n = 12$ ) in response to von Frey hair stimulation of the injured hindpaw, compared with presurgery levels, which averaged  $72.7 \pm 3.7$  mN ( $n = 12$ ). Almost complete ( $\sim 90\%$ ) reversal of tactile hypersensitivity was observed 1 h after systemic administration of (R)-7 ( $10$  mg/kg, ip) (Figure 11B). In contrast, systemic administration of (R)-11 ( $10$  mg/kg, ip) was ineffective at reducing hypersensitivity, with levels averaging  $40 \pm 4.9$  mN ( $n = 6$ ). Neither drug administered systemically to control animals had any effect on paw withdrawal threshold (data not shown).

Mechanical withdrawal threshold changes persisted for all animals ( $n = 12$ ) 4 weeks after TNI (Figure 11B). Systemic administration of (R)-7 ( $10$  mg/kg, ip) partially reversed tactile hypersensitivity at 1 and 4 h after injection. By 24 h, mechanical withdrawal thresholds had returned to predrug levels. Both systemic administration of (R)-11 ( $10$  mg/kg, ip) and morphine sulfate ( $10$  mg/kg, ip) were ineffective at 28 days. The lack of effect of morphine in our study is consistent with a previous report in which neither single doses nor repeated delivery of morphine had much effect on pain-related behavior due to spared-nerve injury model.<sup>46</sup>

Interestingly, we found that  $10$  mg/kg (R)-7 given ip completely reversed TNI-induced hypersensitivity while the same

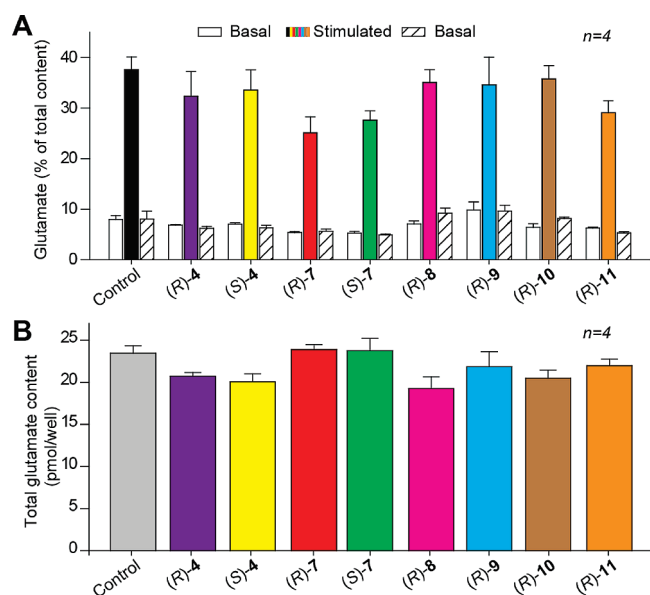


**Figure 9.** Depolarization-induced glutamate release is not affected by 1 compounds. (A) Bar graph of glutamate release expressed as mean percent total glutamate content of cells in each well  $\pm$  SEM ( $n = 4$  wells per condition). Glutamate release was measured from cells treated with successive incubations of normal nondepolarizing HEPES buffer containing 2.5 mM KCl (basal), depolarizing HEPES buffer containing 90 mM KCl (stimulated), and nondepolarizing HEPES buffer containing 2.5 mM KCl again. Poststimulation basal release was not more than 5% different from initial basal levels, indicating that exposure to high extracellular potassium did not damage the cells or induce cell lysis. In all cases, release stimulated by high extracellular  $K^+$  was significantly higher than basal release. However, there were no significant differences in stimulated release between control and any of the drug conditions ( $p > 0.05$ , ANOVA with a Tukey's posthoc test). (B) Total content of glutamate was measured at the end of the release experiment. There were no significant differences in total glutamate content between control and any of the drug conditions ( $p > 0.05$ , ANOVA with a Tukey's posthoc test).

dose of (R)-11 had no effect. This difference was observed despite (R)-7 and (R)-11 displaying similar effects on total  $Na^+$  current and VGSC slow inactivation. In contrast, a pronounced hyperpolarizing shift in voltage-dependent fast inactivation was observed for 30  $\mu$ M (R)-7 (21.4 mV in  $V_{1/2}$ ) compared with a more modest change for 30  $\mu$ M (R)-11 (8.0 mV in  $V_{1/2}$ ). Such a shift in the voltage-dependence of inactivation could lead to decreased neuronal excitability, and this decreased excitability of sensory neurons could be the cause of the antinociceptive effect. Shifts in fast inactivation have been linked to altered excitability and VGSC-related pathology. For example, in myopathy characterized by loss of excitability, it is thought that a similar shift in fast inactivation of muscle VGSC is responsible for muscle fiber excitability.<sup>47,48</sup> Additionally, several mutations in VGSCs associated with chronic pain are known to cause depolarizing shifts in voltage dependence of fast inactivation.<sup>49</sup> These studies highlight how alterations in voltage dependence of fast inactivation can be important for excitability and VGSC-related pathology. It is not surprising, then, that VGSC antagonists (e.g., carbamazepine, lidocaine) have shown efficacy in treating neuropathic pain, likely, in part, by shifting the  $V_{1/2}$  of fast inactivation.<sup>23,50,51</sup> These findings suggest that (R)-7 may reduce excitability by shifting the voltage dependence of fast inactivation and thus

**Table 3.** Veratridine-Induced Glutamate Release Is Not Affected by 1 Compounds

| treatment           | evoked release (% content/15 min) <sup>a</sup> |
|---------------------|--|
| control (0.1% DMSO) | 45.8 $\pm$ 1.6 ( $n = 6$ )                     |
| (R)-4 <sup>b</sup>  | 46.7 $\pm$ 4.7 ( $n = 5$ )                     |
| (R)-7               | 45.7 $\pm$ 0.6 ( $n = 6$ )                     |
| (S)-7               | 50.0 $\pm$ 0.5 ( $n = 5$ )                     |
| (R)-8               | 48.9 $\pm$ 0.6 ( $n = 5$ )                     |
| (R)-9               | 43.6 $\pm$ 1.9 ( $n = 5$ )                     |
| (R)-10              | 47.6 $\pm$ 7.7 ( $n = 5$ )                     |
| (R)-11              | 58.0 $\pm$ 1.0 ( $n = 6$ )                     |

<sup>a</sup> Evoked release, the difference between veratridine-stimulated minus initial basal releases, was normalized to the total content of glutamate over a 15 min period. The total content of glutamate was measured at the end of the release experiment. There were no significant differences in evoked release between control and any of the drug conditions ( $p > 0.05$ , ANOVA with a Tukey's post hoc test). <sup>b</sup> 100  $\mu$ M of (R)-4 or 1 agents was separately added to neurons 30 min prior to the initial basal and maintained throughout the basal (10 min) and stimulated (15 min) measurements.

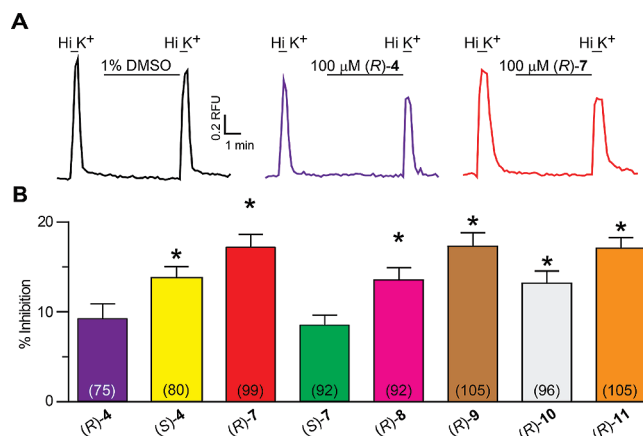


**Figure 10.** Modest inhibition of depolarization-induced  $Ca^{2+}$  influx by 1 compounds in cortical neurons. (A)  $Ca^{2+}$  imaging was performed on E18 rat cortical neurons using the ratiometric  $Ca^{2+}$ -sensitive dye Fura-2. Following a 1 min baseline measurement, neurons were stimulated with 46.5 mM KCl for 30–40 s to induce  $Ca^{2+}$  influx. Neurons were gently washed and then treated singly with drugs (1% DMSO or 100  $\mu$ M compound) for 5 min before stimulating again with 46.5 mM KCl. Representative traces from the indicated treatment groups are shown. (B) Bar graph shows the percent inhibition (adjusted for nonspecific inhibition by DMSO) for the 1 compounds. Values represent the average  $\pm$  SEM from two separate imaging experiments, with the number of cells per condition indicated in parentheses. Asterisks (\*) indicate statistical significance compared with (R)-4 by one-way ANOVA followed by Dunnett's posthoc test  $p < 0.05$ . RFU = relative fluorescence units.

abolish TNI-induced hypersensitivity, along with its effect on sodium channel slow inactivation. An alternative possibility could be that, like the newly discovered organic compound Z123212 reported by Snutch and colleagues,<sup>52</sup> (R)-7 abolishes TNI-induced hypersensitivity through a mechanism of enhancing not only  $Na^+$  channels but T-type  $Ca^{2+}$  channels as well. It is also possible that differences in protein-binding of (R)-7 and (R)-11 as well as the free fractions of (R)-7 and (R)-11 that are

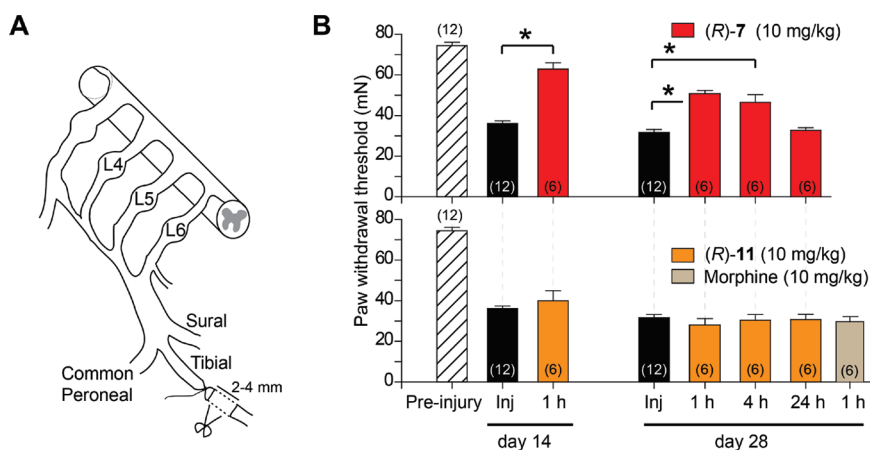


**Figure 11.** (*R*)-7, but not (*R*)-11, reverses mechanical hypersensitivity in the TNI model of neuropathic pain. (A) Diagram of the sural, tibial, and common peroneal terminal nerve branches of the sciatic nerve and their dorsal root origins. Neuropathic pain was induced by ligation of the tibial nerve and 2–4 mm of the nerve distal to the ligation was removed. (B) Withdrawal threshold (in milli-Newtons, mN) in response to von Frey stimulation to the paw ipsilateral to TNI following a single, intraperitoneal administration of (*R*)-7 or (*R*)-11 (10 mg/kg,  $n = 6$ ) at 2 and 4 weeks after injury. A single injection of (*R*)-7 almost completely reversed TNI-induced mechanical hypersensitivity ( $p < 0.05$ ; Student's *t*-test) compared with injured animals that did not receive (*R*)-7. At 4 weeks, the ability of (*R*)-7 to reverse TNI-induced mechanical hypersensitivity was diminished but remained significantly different from vehicle control animals. Neither (*R*)-11 at 2 and 4 weeks after injury or morphine (10 mg/kg) administered at 4 weeks changed the TNI induced pain behavior.

available for pharmacological actions may account for their differential effects on TNI.

The results from the TNI model for (*R*)-7 and (*R*)-11 were compared with findings from the mouse (*ip*) formalin-induced pain model, conducted at the NINDS ASP (data not shown). (*R*)-7 showed potent protection against chronic (late-phase) inflammatory pain (15 mg/kg: 44% protection vs control), while (*R*)-11 displayed no detectable protection (12 mg/kg: 97% protection vs control). In this test protocol, the lower the observed percent protection versus control, the more effective the compound is in preventing neuropathic pain. Recently, Vissers and co-workers demonstrated a good correlation between findings in the chronic phase of the formalin test and results for cold allodynia in the chronic constriction injury model for rats ( $r = 0.72$ ) and gerbils ( $r = 0.68$ ) using drugs with proven pain-attenuating effects in humans.<sup>53</sup>

## CONCLUSIONS

Chimeric agents **1** were formed by merging the structures of functionalized amino acids (**2**) and  $\alpha$ -amino acid amides (**3**) with the expectation that the new compounds would retain pharmacological properties observed for both **2** and **3**. This appears to be the case. Chimeric **1** showed excellent anticonvulsant activities in seizure models comparable with and in some cases exceeding (*R*)-**4** and (*S*)-**5** ((*S*)-**6**). When we examined **1** activities on sodium channel function by whole-cell patch-clamp electrophysiology using CAD cells, we observed that that they were uniformly more potent (16–53-fold) than (*R*)-**4** in facilitating slow inactivation (Table 1). Interestingly, we found a marked increase in state-dependent block and an increase in the level of fast inactivation accompanied the change. Notably, (*R*)-**4** showed preferential inactivation of slow inactivation,<sup>22</sup> and (*S*)-**5**<sup>13,24</sup> and (*S*)-**6**<sup>15</sup> both modulated fast inactivation. The extent of fast inactivation depended on the 4' structural unit in the chimeric **1** agents. For (*R*)-**7**, into which we placed a (3''-fluorophenyl)methoxy unit at the 4' position, we observed a significant increase in fast inactivation compared with

(*R*)-**11**, into which we placed a 3''-fluorophenyl moiety. While the structural moiety at the 4' position did not appreciably affect the slow inactivation properties of the chimeric **1**s or their anticonvulsant activities, they did dramatically influence their antinociceptive properties in the rat-TNI model. Administration of (*R*)-**7** led to complete reversal of evoked pain, while (*R*)-**11** had no detectable effect. Future studies will explore the possible role of the dual promotion of slow and fast sodium channel inactivation processes for novel chimeric **1** agents in this and related neuropathic pain models.

## METHODS

**Chemistry.** Preparation of 4-((2'-Fluorophenoxy)methyl)benzotrile (**14**). A mixture of **12** (25.00 g, 127.5 mmol),  $K_2CO_3$  (425.20 g, 400.0 mmol), and **13** (11.90 g, 106.3 mmol) was heated at reflux in acetone (400 mL) (4 h). The volatiles were evaporated, and the residue was diluted with  $CH_2Cl_2$  (300 mL). The organic layer was washed with  $H_2O$  (300 mL), dried ( $MgSO_4$ ), and concentrated in vacuo to give white needles (19.21 g, 86%):  $R_f = 0.28$  (hexanes/ethyl acetate 9/1); mp 69–70 °C;  $^1H$  NMR ( $CDCl_3$ )  $\delta$  5.19 (s,  $CH_2O$ ), 6.91–7.14 (m, 2 ArH), 7.01–7.14 (m, 2 ArH), 7.56 (d,  $J = 7.8$  Hz, 2 ArH), 7.67 (d,  $J = 7.8$  Hz, 2 ArH);  $^{13}C$  NMR ( $CDCl_3$ )  $\delta$  70.3 ( $CH_2O$ ), 111.8 (CCN), 115.8 ( $C_{6'}$ ), 116.5 (d,  $J = 18.6$  Hz,  $C_{3'}$ ), 118.6 (CN), 122.2 (d,  $J = 6.9$  Hz,  $C_{5'}$  or  $C_{4'}$ ), 124.3 (d,  $J = 3.8$  Hz,  $C_{5'}$  or  $C_{4'}$ ), 127.5, 132.4, 142.0 (3Ar), 146.2 (d,  $J = 10.9$  Hz,  $C_{1'}$ ), 152.9 (d,  $J = 244.7$  Hz,  $C_{2'}$ ); HRMS ( $M + H^+$ ) ( $ESI^+$ ) not observed [ $M + H^+$ ] (calcd for  $C_{14}H_{10}FNOH^+$  228.0825).

Preparation of 4-((2'-Fluorophenoxy)methyl)benzylamine (**15**). To a  $LiAlH_4$  (4.75 g, 198.2 mmol) suspension in tetrahydrofuran (THF; 600 mL) was added dropwise at 0 °C a THF (30 mL) solution of **14** (15.00 g, 66.1 mmol). The mixture was stirred at room temperature (16 h). Then,  $H_2O$  (6 mL) was added dropwise at 0 °C followed by an aqueous NaOH solution (3 mL, 15% w/w) and  $H_2O$  (6 mL). The mixture was stirred at room temperature (2 h), and the precipitate was filtered and the pad was washed with  $CH_2Cl_2$ . The filtrate was concentrated in vacuo to obtain 11.20 g (73%) of **15** as a colorless oil:  $R_f = 0.00$  (hexanes/ $EtOAc$  9/1);  $^1H$  NMR ( $CDCl_3$ )  $\delta$  1.65 (br s,  $NH_2$ ),

3.86 (s, CH<sub>2</sub>NH<sub>2</sub>), 5.11 (s, CH<sub>2</sub>O), 6.85–7.20 (m, 4 ArH), 7.31 (d, *J* = 8.0 Hz, 2 ArH), 7.40 (d, *J* = 8.0 Hz, 2 ArH); <sup>13</sup>C NMR (CDCl<sub>3</sub>) δ 46.2 (CH<sub>2</sub>NH<sub>3</sub>), 71.2 (CH<sub>2</sub>O), 115.8 (d, *J* = 2.3 Hz, C<sub>6'</sub>), 116.9 (d, *J* = 17.8 Hz, C<sub>3'</sub>), 121.5 (d, *J* = 6.2 Hz, C<sub>5'</sub> or C<sub>4'</sub>), 124.2 (d, *J* = 4.6 Hz, C<sub>5'</sub> or C<sub>4'</sub>), 127.7, 127.8, 135.9, 137.7 (4 Ar), 146.6 (d, *J* = 10.8 Hz, C<sub>1'</sub>), 152.9 (d, *J* = 244.7 Hz, C<sub>2'</sub>); HRMS (*M* + H<sup>+</sup>) (ESI<sup>+</sup>) 232.1138 [*M* + H<sup>+</sup>] (calcd for C<sub>14</sub>H<sub>14</sub>FNOH<sup>+</sup> 232.1137).

**Preparation of (*R*)-*N*-4'-((2''-Fluorophenoxy)methyl)benzyl 2-*N*-(*tert*-butoxycarbonyl)amino-3-hydroxypropionamide ((*R*)-**17**).** A THF solution (250 mL) of (*R*)-**16** (5.00 g, 21.6 mmol) was stirred and cooled at –78 °C under Ar, and then 4-methylmorpholine (NMM) (2.9 mL, 26.0 mmol) was added dropwise. After 2 min of stirring at this temperature, isobutylchloroformate (IBCF) (3.4 mL, 26.0 mmol) was added dropwise leading to the precipitation of a white solid, and the reaction was allowed to proceed for additional 2 min, and then **15** (6.00 g, 26.0 mmol) was added portionwise at –78 °C. The mixture was allowed to stir at room temperature (2 h), and the white solid filtered and the organic layer concentrated in vacuo. The residue was purified by flash column chromatography on silica gel with EtOAc/hexanes (5/5 to 8/0) as the eluant to obtain (*R*)-**17** as a white solid (8.10 g, 90%): *R*<sub>f</sub> = 0.36 (hexanes/EtOAc 5/5); mp 64–67 °C; [α]<sup>25.2</sup><sub>D</sub> +31.2° (*c* 0.5, CHCl<sub>3</sub>); IR (crystal) 3327, 3003, 2943, 1734, 1686, 1651, 1557, 1522, 1508, 1454, 1445, 1366, 1261, 1229, 1217, 1206, 1165, 1109, 1034, 1007, 792 cm<sup>-1</sup>; <sup>1</sup>H NMR (400 MHz, CDCl<sub>3</sub>) δ 1.41 (s, (CH<sub>3</sub>)<sub>3</sub>), 3.15–3.42 (br m, OH), 3.61–3.73 (br m, CHH'), 4.02–4.21 (br m, CHH', CH), 4.30–4.58 (br m, CH<sub>2</sub>NH), 5.09 (s, OCH<sub>2</sub>), 5.54–5.68 (br t, NH), 6.87–7.16 (m, 4 ArH, NH), 7.24–7.29 (m, 2 ArH), 7.36–7.40 (m, 2 ArH); <sup>13</sup>C NMR (100 MHz, CDCl<sub>3</sub>) δ 28.2 ((CH<sub>3</sub>)<sub>3</sub>), 43.1 (NCH<sub>2</sub>), 54.8 (OCH<sub>2</sub>CH), 62.8 (OCH<sub>2</sub>CH), 71.0 (OCH<sub>2</sub>), 80.6 (C(CH<sub>3</sub>)<sub>3</sub>), 115.7 (C<sub>6'</sub>), 116.3 (d, *J* = 17.8 Hz, C<sub>3'</sub>), 121.4 (d, *J* = 6.9 Hz, C<sub>5'</sub> or C<sub>4'</sub>), 124.2 (d, *J* = 3.9 Hz, C<sub>5'</sub> or C<sub>4'</sub>), 127.3, 127.7, 135.1, 143.2 (4 Ar), 146.7 (d, *J* = 10.8 Hz, C<sub>1'</sub>), 153.0 (d, *J* = 243.9 Hz, C<sub>2'</sub>), 156.3 (NHC(O)O), 171.4 (C(O)); HRMS (*M* + Na<sup>+</sup>) (ESI<sup>+</sup>) 441.1802 [*M* + Na<sup>+</sup>] (calcd for C<sub>22</sub>H<sub>28</sub>N<sub>2</sub>O<sub>5</sub>Na<sup>+</sup> 442.1874). Anal. Calcd. for C<sub>22</sub>H<sub>28</sub>N<sub>2</sub>O<sub>5</sub>: C, 63.14; H, 6.50; F, 4.54; N, 6.69. Found: C, 62.86; H, 6.57; F, 4.34; N, 6.88.

**Preparation of (*R*)-*N*-4'-((2''-Fluorophenoxy)methyl)benzyl 2-*N*-(*tert*-butoxycarbonyl)amino-3-methoxypropionamide ((*R*)-**18**).** Ag<sub>2</sub>O (20.44 g, 88.5 mmol) was added to a CH<sub>3</sub>CN solution (450 mL) of (*R*)-**17** (7.40 g, 17.7 mmol) and CH<sub>3</sub>I (11.0 mL, 177.0 mmol) at room temperature under Ar. The reaction mixture was stirred at room temperature in the dark (3 d) and filtered through Celite, and the filtrate concentrated in vacuo to obtain a white solid. The solid was purified by flash column chromatography on silica gel with EtOAc/hexanes (3/7 to 6/4) as the eluant to obtain (*R*)-**18** as a white solid (5.00 g, 65%): *R*<sub>f</sub> = 0.61 (EtOAc/hexanes 1/1); mp 103–104 °C; [α]<sup>25.9</sup><sub>D</sub> –16.5° (*c* 0.5, CHCl<sub>3</sub>); IR (crystal) 3370, 1695, 1682, 1647, 1547, 1524, 1504, 1460, 1391, 1364, 1317, 1277, 1254, 1198, 1167, 1109, 1086, 1045, 1018, 1001 cm<sup>-1</sup>; <sup>1</sup>H NMR (400 MHz, CDCl<sub>3</sub>) δ 1.43 (s, (CH<sub>3</sub>)<sub>3</sub>C), 3.37 (s, CH<sub>3</sub>), 3.48–3.51 (br m, CHH'), 3.84 (dd, *J* = 3.2, 5.6 Hz, CHH'), 4.22–4.29 (m, CH), 4.41–4.53 (m, CH<sub>2</sub>NH), 5.12 (s, OCH<sub>2</sub>), 5.32–5.44 (br m, NH), 6.68–6.76 (br m, NH), 6.89–7.14 (m, 4 ArH), 7.28 (d, *J* = 8.2 Hz, 2 ArH), 7.40 (d, *J* = 8.2 Hz, 2 ArH); <sup>13</sup>C NMR (100 MHz, CDCl<sub>3</sub>) δ 28.2 ((CH<sub>3</sub>)<sub>3</sub>), 43.1 (NCH<sub>2</sub>), 54.0 (OCH<sub>2</sub>CH), 56.1 (OCH<sub>3</sub>), 71.0, 72.0 (2 OCH<sub>2</sub>), 80.5 (C(CH<sub>3</sub>)<sub>3</sub>), 115.7 (d, *J* = 1.6 Hz, C<sub>6'</sub>), 116.3 (d, *J* = 17.8 Hz, C<sub>3'</sub>), 121.5 (d, *J* = 7.0 Hz, C<sub>5'</sub> or C<sub>4'</sub>), 124.2 (d, *J* = 3.9 Hz, C<sub>5'</sub> or C<sub>4'</sub>), 127.7, 127.8, 135.8, 137.9 (4 ArH), 146.6 (d, *J* = 10.8 Hz, C<sub>1'</sub>), 152.9 (d, *J* = 244.7 Hz, C<sub>2'</sub>), 155.5 (NHC(O)O), 170.3 (C(O)); HRMS (*M* + Na<sup>+</sup>) (ESI<sup>+</sup>) 455.1958 [*M* + Na<sup>+</sup>] (calcd for C<sub>23</sub>H<sub>29</sub>FN<sub>2</sub>O<sub>5</sub>Na<sup>+</sup> 455.1952). Anal. Calcd. for C<sub>23</sub>H<sub>29</sub>FN<sub>2</sub>O<sub>5</sub>: C, 63.87; H, 6.76; F, 4.39; N, 6.48. Found: C, 64.01; H, 6.85; F, 4.31; N, 6.56.

**Preparation of (*R*)-*N*-4'-((2''-Fluorophenoxy)methyl)benzyl 2-*acet*-amido-3-methoxypropionamide ((*R*)-**10**).** A saturated HCl solution in

dioxane (1 mmol/2 mL, 22.2 mL) was added to an Et<sub>2</sub>O (10 mL) solution of (*R*)-**18** (4.50 g, 11.1 mmol) at 0 °C, and the solution was stirred at room temperature (16 h). The reaction solution was concentrated in vacuo and dried (30 min).

The residue was dissolved in CH<sub>2</sub>Cl<sub>2</sub> (60 mL), and Et<sub>3</sub>N (4.7 mL, 33.3 mmol) and AcCl (1.2 mL, 16.7 mmol) were successively added at 0 °C. The mixture was stirred at room temperature (16 h), aqueous 10% citric acid (60 mL) was added, and then the organic layer was separated. The aqueous layer was washed with CH<sub>2</sub>Cl<sub>2</sub> (2 × 30 mL). All of the organic layers were combined, washed with aqueous saturated NaHCO<sub>3</sub> (30 mL) and H<sub>2</sub>O (30 mL), dried (MgSO<sub>4</sub>), and concentrated in vacuo. The solid was recrystallized with EtOAc to obtain (*R*)-**10** as a white solid (2.40 g, 58%): *R*<sub>f</sub> = 0.31 (EtOAc); mp 149 °C; [α]<sup>25.3</sup><sub>D</sub> –20.2° (*c* 0.5, CHCl<sub>3</sub>); IR (crystal) 3281, 1645, 1549, 1506, 1456, 1433, 1375, 1312, 1281, 1261, 1231, 1198, 1111, 1097, 1040, 1001, 989 cm<sup>-1</sup>; <sup>1</sup>H NMR (400 MHz, CDCl<sub>3</sub>) δ 2.03 (s, CH<sub>3</sub>C(O)), 3.37 (s, CH<sub>3</sub>), 3.40–3.45 (br m, CHH'), 3.80–3.83 (m, CHH'), 4.46–4.54 (m, CH, CH<sub>2</sub>NH), 5.12 (s, OCH<sub>2</sub>), 6.40 (br d, *J* = 4.8 Hz, NH), 6.71–6.78 (br m, NH), 6.90–7.14 (m, 4 ArH), 7.27 (d, *J* = 6.8 Hz, 2 ArH), 7.41 (d, *J* = 6.8 Hz, 2 ArH), addition of excess (*R*)-(-)-mandelic acid to a CDCl<sub>3</sub> solution of (*R*)-**10** gave only one signal for the acetyl methyl and one signal for the ether methyl protons; <sup>13</sup>C NMR (100 MHz, CDCl<sub>3</sub>) δ 28.2 (CH<sub>3</sub>(O)), 43.2 (NCH<sub>2</sub>), 52.4 (OCH<sub>2</sub>CH), 59.1 (OCH<sub>3</sub>), 71.0, 71.7 (2 OCH<sub>2</sub>), 115.7 (d, *J* = 1.5 Hz, C<sub>6'</sub>), 116.3 (d, *J* = 18.6 Hz, C<sub>3'</sub>), 121.5 (d, *J* = 7.0 Hz, C<sub>5'</sub> or C<sub>4'</sub>), 124.2 (d, *J* = 3.9 Hz, C<sub>5'</sub> or C<sub>4'</sub>), 127.7, 127.8, 135.9, 137.8 (4 Ar), 146.6 (d, *J* = 10.1 Hz, C<sub>1'</sub>), 152.9 (d, *J* = 244.7 Hz, C<sub>2'</sub>), 170.0, 170.3 (2 C(O)); HRMS (*M* + Na<sup>+</sup>) (ESI<sup>+</sup>) 397.1540 [*M* + Na<sup>+</sup>] (calcd for C<sub>20</sub>H<sub>23</sub>FN<sub>2</sub>O<sub>4</sub>Na<sup>+</sup> 397.1534). Anal. Calcd. for C<sub>20</sub>H<sub>23</sub>FN<sub>2</sub>O<sub>4</sub>: C, 64.16; H, 6.19; F, 5.07; N, 7.48. Found: C, 64.01; H, 6.14; F, 4.91; N, 7.55.

**Electrophysiology.** Whole-cell voltage clamp recordings were performed at room temperature on CAD cells using an EPC 10 amplifier (HEKA Electronics, Germany). Electrodes were pulled from thin-walled borosilicate glass capillaries (Warner Instruments, Hamden, CT) with a P-97 electrode puller (Sutter Instrument, Novato, CA) such that final electrode resistances were 1–2 MΩ when filled with internal solutions. The internal solution for recording Na<sup>+</sup> currents contained (in mM) 110 CsCl, 5 MgSO<sub>4</sub>, 10 EGTA, 4 ATP Na<sub>2</sub>-ATP, and 25 HEPES (pH 7.2, 290–310 mOsm/L). The external solution contained (in mM) 100 NaCl, 10 tetraethylammonium chloride (TEA-Cl), 1 CaCl<sub>2</sub>, 1 CdCl<sub>2</sub>, 1 MgCl<sub>2</sub>, 10 D-glucose, 4 4-AP, 0.1 NiCl<sub>2</sub>, and 10 HEPES (pH 7.3, 310–315 mOsm/L). Whole-cell capacitance and series resistance were compensated with the amplifier. Series resistance error was always compensated to be less than ±3 mV. Cells were considered only when the seal resistance was less than 3 MΩ. Linear leak currents were digitally subtracted by P/4. To negate any potential effects of time-dependent shifts in the voltage dependence of fast inactivation, we compared data obtained 3–4 min after establishing the whole-cell recording configuration from cells without drug against cells with the **1** agents.

**Data Acquisition and Analysis.** Signals were filtered at 10 kHz and digitized at 10–20 kHz. Analysis was performed using Fitmaster and origin8.1 (OriginLab Corporation, Northampton, MA). For activation curves, conductance (*G*) through Na<sup>+</sup> channels was calculated using the equation  $G = I / (V_m - V_{rev})$ , where *V*<sub>rev</sub> is the reversal potential, *V*<sub>m</sub> is the membrane potential at which the current was recorded, and *I* is the peak current. Activation and inactivation curves were fitted to a single-phase Boltzmann function  $G/G_{max} = 1 / \{1 + \exp[(V - V_{50})/k]\}$ , where *G* is the peak conductance, *G*<sub>max</sub> is the fitted maximal *G*, *V*<sub>50</sub> is the half-activation voltage, and *k* is the slope factor. Additional details of specific pulse protocols are described in the results text or figure legends.

**Potassium Chloride- or Veratridine-Induced Glutamate Release.** Glutamate released from embryonic cortical neurons was measured using the Amplex Red glutamic acid/glutamate oxidase assay kit (Invitrogen) as described previously.<sup>54,55</sup> In this assay, L-glutamic

acid is oxidized by glutamate oxidase to produce  $\alpha$ -ketoglutarate,  $\text{NH}_3$ , and  $\text{H}_2\text{O}_2$ .  $\text{H}_2\text{O}_2$  reacts with the Amplex Red reagent in a 1:1 stoichiometry in a reaction catalyzed by horseradish peroxidase (HRP) to generate the highly fluorescent product resorufin. After 30 min, fluorescence of resorufin was measured in a Victor<sup>3</sup> V multilabel plate reader (Perkin-Elmer, Shelton, CT) using excitation at 530 nm and emission at 590 nm.

To generate samples, neurons growing in 12-well plates were washed three times (300  $\mu\text{L}$  each) with nondepolarizing buffer (119 mM NaCl, 2.5 mM KCl, 2 mM  $\text{CaCl}_2$ , 2 mM  $\text{MgCl}_2$ , 25 mM HEPES, and 30 mM D-glucose). A 100  $\mu\text{L}$  sample was collected after the third wash for basal samples. After a 15 min stimulation with depolarizing buffer (32 mM NaCl, 90 mM KCl, 2 mM  $\text{CaCl}_2$ , 2 mM  $\text{MgCl}_2$ , 25 mM HEPES, and 30 mM D-glucose), 100  $\mu\text{L}$  of culture supernatant was collected and stored at  $-20^\circ\text{C}$ . Finally, neurons were bathed in nondepolarizing buffer for 15 min to re-establish resting levels. For veratridine release experiments, 100  $\mu\text{M}$  veratridine was used as the stimulus in nondepolarizing buffer. Then 100  $\mu\text{M}$  of (R)-4 or 1 agents were separately added to neurons 30 min prior to the initial basal and maintained throughout the basal (10 min) and stimulated (10 min) measurements. The nontransportable glutamate transporter inhibitor DL-threo- $\beta$ -benzyloxaspartate (DL-TBOA; 500  $\mu\text{M}$ ) was present during the stimulation to prevent reuptake of released glutamate.<sup>55</sup> The remaining glutamate content in each well was determined by exposing the cells to 2% Triton X-100 in nondepolarizing buffer. Total content levels represent the sum of the remaining glutamate content with the previously collected fractions. The glutamate released during the 15 min stimulation period is expressed as percent of the total content. Standard curves for the assay with known concentrations of exogenous glutamate demonstrated high reproducibility and sensitivity of the assay, with a lower limit of detection of  $\sim 15$  fmol glutamate. Standard curves were constructed for each assay. The concentrations of  $\text{K}^+$  and time period for stimulation were chosen because they lie on the middle of the sloped portion of the concentration response curve for KCl-stimulated glutamate release. In additional control experiments, the general  $\text{Ca}^{2+}$  channel blocker  $\text{CdCl}_2$  (500  $\mu\text{M}$ ) blocked basal and  $\text{K}^+$ -stimulated glutamate release (not shown).

**Fluorescent Calcium Imaging.** Changes in internal calcium were monitored using the  $\text{Ca}^{2+}$  sensitive dye Fura-2AM (Invitrogen, Carlsbad, CA). E18 neurons grown in culture for four days were loaded with 3  $\mu\text{M}$  Fura-2AM (in nondepolarizing Hepes buffer; 119 NaCl, 2.5 KCl, 2  $\text{CaCl}_2$ , 2  $\text{MgCl}_2$ , 25 HEPES pH 7.5, 30 glucose, concentrations in mM) for 25 min at room temperature protected from light. Neurons were then washed thrice with buffer and transferred to the imaging stage. Neurons loaded with the cell permeable Fura-2AM were visualized by differential interference contrast at  $20\times$  for a field of view containing  $\sim 70$  neurons. After a 1 min baseline of ratiometric fluorescent units (RFUs) was obtained, neurons were stimulated with 46.5 mM KCl for 30–40 s and then washed in normal nondepolarizing Hepes buffer, which allowed a return to baseline RFUs. Cell fluorescence was measured by digital video microfluorometry with an intensified CCD camera coupled to a microscope and Nikon Elements software (Nikon Instruments Inc., Melville, NY). Cells were illuminated with a Lambda DG-4 175 W xenon lamp, and the excitation wavelengths of Fura-2 (340/380 nm) were selected by a filter changer. Fura-2 fluorescence ( $F_{340}/F_{380}$ ) was measured every 10 s to minimize photobleaching. After a baseline of at least six images was obtained, neurons were stimulated by exposure to 46.5 mM KCl (peak 1, P1) for 30–40 s, leading to a sharp increase in  $F_{340}/F_{380}$  which returned to baseline levels when KCl was removed. Neurons were then treated for 5 min with vehicle or drug prior to being stimulated again with 46.5 mM KCl (peak 2, P2) as before. Only cells that displayed a P1 ratio that was 2-fold greater than baseline were used to determine the inhibitory effect of the drugs. After subtracting baseline values, inhibition was calculated using the following equation % inhibition =  $100 \times [(P2 - P1)/P1]$ .

**Tibial-Nerve Injury.** All procedures were performed on adult (150–200 g) female Sprague–Dawley rats. The experiments were approved by the Animal Care Committee of the Indiana University School of Medicine and followed IASP ethical guidelines.

Under isoflurane (2%) anesthesia, the skin on the lateral surface of the thigh was incised and a section made directly through the biceps femoris muscle exposing the sciatic nerve and its three terminal branches: the sural, common peroneal and tibial nerves. The surgical procedure comprised an axotomy and ligation of the tibial nerve leaving the common peroneal and sural nerves intact. The tibial nerve was tightly ligated with 5.0 silk and sectioned distal to the ligation, removing 2–4 mm of the distal nerve stump (Figure 11A). Effort was made to avoid contact with or stretching of the intact common peroneal and sural nerves. Muscle and skin were closed in two layers. Sham controls involved exposure of the sciatic nerve and its branches without any lesion.

**Behavior: Foot Withdrawal to Punctate Mechanical Indentation.** Sixteen animals were divided into two groups: twelve animals with a tibial nerve injury and four sham control animals. The animals were tested for behavioral responsiveness after 3 days of habituation to the testing environment and observer. Behavioral baseline measurements were collected from at least 2 separate days prior to the surgery. The rats were then tested 7 days after the surgery and weekly thereafter.

The incidence of foot withdrawal was measured in response to mechanical indentation of the plantar surface of each hind paw with custom Von Frey-type filaments. Mechanical stimuli were applied with seven filaments, each differing in the bending force delivered (10, 20, 40, 60, 80, 100, and 120 mN), but each fitted with the same metal cylinder with a flat tip and a fixed diameter of 0.2 mm. The filaments will be applied in order of ascending force. Each filament was applied to the foot ipsilateral to the nerve injury. The duration of each stimulus was approximately 1 s followed by an interstimulus interval of approximately 10–15 s. The incidence of foot withdrawal was expressed as a percentage of the six applications of each stimulus and the percentage of withdrawals was then plotted as a function of force. The von Frey withdrawal threshold was defined as the force that evoked a minimum detectable withdrawal observed on 50% of the tests given at the same force level. For cases in which none of the specific filaments used evoked withdrawals on exactly 50% of the tests, linear interpolation will be used to define the threshold.

The incidence of foot withdrawal was expressed as a percentage of the six applications of each filament as a function of force. A Hill equation was fitted to the function (Origin version 6.0, Microcal Software, Northampton MA) relating the percentage of indentations eliciting a withdrawal to the force of indentation. From this equation, the paw withdrawal threshold (PWT) force was obtained and defined as the force corresponding to a 50% withdrawal. In each behavioral testing sequence, the operator was blinded to the animal treatment condition.

**Drugs and Drug Administration.** Morphine sulfate salt was provided from NIDA Drug Supply Program (Rockville, MD). Systemic morphine or vehicle was administered by intraperitoneal injection in a volume of 250  $\mu\text{L}$ . (R)-7 and (R)-11 were employed in this model. Both compounds were freshly prepared in saline (0.5% DMSO) on the day of the experiment (10 mg/kg). (R)-7 ( $n = 6$ ) and (R)-11 ( $n = 6$ ) were administered as a one-time intraperitoneal (ip) injection 1 h prior to behavioral testing. Sham control animals also were treated with 10 mg/kg dose of (R)-7 ( $n = 2$ ) and (R)-11 ( $n = 2$ ).

Animals were randomly assigned to the two drug treatment groups. Results are presented as mean  $\pm$  SEM. The data were analyzed by one-way ANOVA and Bonferroni posthoc tests. A  $p$  value of  $<0.05$  was accepted as significant.

**Statistical Analyses.** Differences between means were compared by either paired or unpaired, two-tailed Student's  $t$ -tests or an analysis of

variance (ANOVA) when comparing multiple groups (repeated measures whenever possible). If a significant difference was determined by ANOVA, then a Dunnett's or Tukey's posthoc test was performed. Data are expressed as mean  $\pm$  SEM, with  $p < 0.05$  considered as the level of significance.

## AUTHOR INFORMATION

### Corresponding Author

\*E-mail: khanna5@iupui.edu (R.K.); harold\_kohn@email.unc.edu (H.K.).

### Author Contributions

<sup>#</sup>These authors contributed equally to the work.

### Author Contributions

Y.W. conducted whole cell electrophysiology. S.W. performed glutamate release experiments and helped in the editing of the manuscript. J.M.B. performed the calcium imaging experiments. M.S.R. performed the tibial-nerve injury and behavior experiments. C.S. and K.D.P. synthesized the compounds. F.A.W. analyzed the behavior data and helped write the injury and behavior sections. R.K. and H.K. conceived the study, designed and supervised the overall project, and wrote the manuscript.

### Funding Sources

This work is supported by grants from the National Institutes of Health (NIH) (RO1NS054112 to H.K.; NS049136 and DA026040 to F.A.W.), Award UL1RR025747 from the National Center for Research Resources (H.K.), the Indiana State Department of Health—Spinal Cord and Brain Injury Fund (A70-9-079138 to R.K.), the Indiana University Biomedical Committee—Research Support Funds (2286501 to R.K.), and the Elwert Award in Medicine to R.K. The work performed at NIMH was supported by NIMH Psychoactive Drug Screening Program, Contract No. HHSN-271-2008-00025-C (NIMH-PDSP). S.M. W. is a Stark Scholar. J.M.B. is the recipient of a Larry Kays Medical Neuroscience fellowship.

## DISCLOSURE

The content is solely the responsibility of the authors and does not represent the official views of the National Center for Research Resources, National Institute of Neurological Disorders and Stroke, or the National Institutes of Health.

### Notes

H.K. has a royalty-stake position in (R)-4, and UNC has filed patent applications in behalf of the compounds in this study.

## ACKNOWLEDGMENT

We thank Dr. Theodore Cummins (SNRI, Indiana University School of Medicine) and Andrew Piekarczyk for discussions and comments on the manuscript. We thank the NINDS and the ASP at the National Institutes of Health with James P. Stables and Drs. Tracy Chen and Jeffrey Jiang for kindly performing the pharmacological studies via the ASP's contract site at the University of Utah with Drs. H. Wolfe, H. S. White, and K. Wilcox. We express our appreciation to Dr. Bryan L. Roth and Mr. Jon Evans at the National Institute of Mental Health (NIMH) Psychoactive Drug Screening Project for performing in vitro receptor binding studies. The NIMH PDSP is directed by Bryan Roth M.D., Ph.

D. at the University of North Carolina at Chapel Hill and Project Officer Jamie Driscoll at NIMH, Bethesda, MD.

## ABBREVIATIONS

FAA, functionalized amino acid; AAA,  $\alpha$ -amino acid amide; AED, antiepileptic drug; TTX-S, tetrodotoxin-sensitive; TNI, tibial-nerve injury; VGSC, voltage-gated  $\text{Na}^+$  channel; CAD, catecholamine A differentiated; SAR, structure—activity relationship;  $\text{Na}_v1.x$ , voltage-gated  $\text{Na}^+$  channel isoform 1.x;  $I_{\text{Na}}$ ,  $\text{Na}^+$  current; MES, maximal electroshock; ASP, Anticonvulsant Screening Program; NINDS, National Institute of Neurological Disorders and Stroke; ip, intraperitoneally; po, orally;  $\text{ED}_{50}$ , 50% effective dose;  $\text{TD}_{50}$ , 50% neurological impairment; scMet, subcutaneous Metrazol; CNS, central nervous system;  $\text{IC}_{50}$ , concentration at which half of the channels have transitioned to a slow inactivated state; NIMH, National Institute of Mental Health

## REFERENCES

- (1) Salomé, C., Salomé-Grosjean, E., Stables, J. P., and Kohn, H. (2010) Merging the structural motifs of functionalized amino acids and  $\alpha$ -aminoamides: Compounds with significant anticonvulsant activities. *J. Med. Chem.* 53, 3756–3771.
- (2) Cortes, S., Liao, Z.-K., Watson, D., and Kohn, H. (1985) Effect of structural modification of the hydantoin ring on anticonvulsant activity. *J. Med. Chem.* 28, 601–606.
- (3) Conley, J. D., and Kohn, H. (1987) Functionalized D,L-amino acid derivatives. Potent new agents for the treatment of epilepsy. *J. Med. Chem.* 30, 567–574.
- (4) Kohn, H., and Conley, J. D. (1988) New antiepileptic agents. *Chem. Br.* 24, 231–234.
- (5) Kohn, H., Conley, J. D., and Leander, J. D. (1988) Marked stereospecificity in a new class of anticonvulsants. *Brain Res.* 457, 371–375.
- (6) Kohn, H., Sawhney, K. N., LeGall, P., Conley, J. D., Robertson, D. W., and Leander, J. D. (1990) Preparation and anticonvulsant activity of a series of functionalized  $\alpha$ -aromatic and  $\alpha$ -heteroaromatic amino acids. *J. Med. Chem.* 33, 919–926.
- (7) Kohn, H., Sawhney, K. N., LeGall, P., Robertson, D. W., and Leander, J. D. (1991) Preparation and anticonvulsant activity of a series of functionalized  $\alpha$ -heteroatom-substituted amino acids. *J. Med. Chem.* 34, 2444–2452.
- (8) Kohn, H., Sawhney, K. N., Bardel, P., Robertson, D. W., and Leander, J. D. (1993) Synthesis and anticonvulsant activities of  $\alpha$ -heterocyclic  $\alpha$ -acetamido-N-benzylacetamide derivatives. *J. Med. Chem.* 36, 3350–3360.
- (9) Bardel, P., Bolanos, A., and Kohn, H. (1994) Synthesis and anticonvulsant activities of  $\alpha$ -acetamido-N-benzylacetamide derivatives containing an electron-deficient  $\alpha$ -heteroaromatic substituent. *J. Med. Chem.* 37, 4567–4571.
- (10) Choi, D., Stables, J. P., and Kohn, H. (1996) Synthesis and anticonvulsant activities of N-benzyl-2-acetamidopropionamide derivatives. *J. Med. Chem.* 39, 1907–1916.
- (11) Pevarello, P., Bonsignori, A., Dostert, P., Heidempergher, F., Pinciroli, V., Colombo, M., McArthur, R. A., Salvati, P., Post, C., Fariello, R. G., and Varasi, M. (1998) Synthesis and anticonvulsant activity of a new class of 2-[(arylalkyl)amino]alkanamide derivatives. *J. Med. Chem.* 41, 579–590.
- (12) Caccia, C., Maj, R., Calabresi, M., Maestroni, S., Faravelli, L., Curatolo, L., Salvati, P., and Fariello, R. G. (2006) Safinamide: From molecular targets to a new anti-Parkinson drug. *Neurology* 67 (7, Suppl. 2), S18–S23.
- (13) Salvati, P., Maj, R., Caccia, C., Cervini, M. A., Fornaretto, M. G., Lamberti, E., Pevarello, P., Skeen, G. A., White, H. S., Wolf, H. H., Faravelli, L., Mazzanti, M., Mancinelli, M., Varasi, M., and Fariello, R. G. (1999) Biochemical and electrophysiological studies on the mechanism

of action of PNU-151774E, a novel antiepileptic compound. *J. Pharmacol. Exp. Ther.* 288, 1151–1159.

(14) Vereroni, O., Maj, R., Calabresi, M., Faravelli, L., Fariello, R. G., and Salvati, P. (2003) Anti-alloodynic effect of NW-1029, a novel Na<sup>+</sup> channel blocker, in experimental animal models of inflammatory and neuropathic pain. *Pain* 102, 17–25.

(15) Stummann, T. C., Salvati, P., Fariello, R. G., and Faravelli, L. (2005) The anti-nociceptive agent ralfinamide inhibits tetrodotoxin-resistant and tetrodotoxin-sensitive Na<sup>+</sup> currents in dorsal root ganglion neurons. *Eur. J. Pharmacol.* 510, 197–208.

(16) Perucca, E., Yasothan, U., Clincke, G., and Kirkpatrick, P. (2008) Lacosamide. *Nat. Rev. Drug Discovery* 7, 973–974.

(17) [http://www.merckserono.com/corp.merckserono/en/images/20101104\\_en\\_tcm112\\_59527.pdf](http://www.merckserono.com/corp.merckserono/en/images/20101104_en_tcm112_59527.pdf).

(18) [http://www.drugs.com/clinical\\_trials/newron-reports-serenatrial-top-line-results-ralfinamide-9336.html](http://www.drugs.com/clinical_trials/newron-reports-serenatrial-top-line-results-ralfinamide-9336.html).

(19) Stoehr, T., Kupferberg, H. J., Stables, J. P., Choi, D., Harris, R. H., Kohn, H., Walton, N., and White, H. S. (2007) Lacosamide, a novel anti-convulsant drug, shows efficacy with a wide safety margin in rodent models for epilepsy. *Epilepsy Res.* 74, 147–154.

(20) Maj, R., Fariello, R., Pevarello, P., Varasi, M., McArthur, R. A., and Salvati, P. (1999) Anticonvulsant activity of PNU-151774E in the amygdala kindled model of complex partial seizures. *Epilepsia* 40, 1523–1528.

(21) Levy, R. H.; Mattson, R.; Meldrum, B. (1995) *Antiepileptic Drugs*, 4th ed., Chapter 6, Raven Press, New York.

(22) Errington, A. C., Stoehr, T., Heers, C., and Lees, G. (2008) The investigational anticonvulsant lacosamide selectively enhances slow inactivation of voltage-gated sodium channels. *Mol. Pharmacol.* 73, 157–169.

(23) Sheets, P. L., Heers, C., Stoehr, T., and Cummis, T. R. (2008) Differential block of sensory neuronal voltage-gated sodium channels by lacosamide [(2R)-2-(acetylamino)-N-benzyl-3-methoxypropanamide], lidocaine, and carbamazepine. *J. Pharmacol. Exp. Ther.* 326, 89–99.

(24) Fariello, R. G. (2007) Safinamide. *Neurotherapeutics* 4, 110–116.

(25) Porter, R. J., Cereghino, J. J., Gladding, G. D., Hessie, B. J., Kupferberg, H. J., Scoville, B., and White, B. G. (1984) Antiepileptic drug development program. *Cleveland Clin. Q.* 51, 293–305.

(26) Wang, H., and Oxford, G. S. (2000) Voltage-dependent ion channels in CAD cells: A catecholaminergic neuronal line that exhibits inducible differentiation. *J. Neurophysiol.* 84, 2888–2895.

(27) Wang, Y., Park, K. D., Salomé, C., Wilson, S. M., Stables, J. P., Liu, R., Khanna, R., and Kohn, H. (2011) Development and characterization of novel derivatives of the antiepileptic drug lacosamide that exhibit far greater enhancement in slow inactivation of voltage-gated sodium channels. *ACS Chem. Neurosci.* 2, 90–106.

(28) Lee, B. H., Won, R., Baik, E. J., Lee, S. H., and Moon, C. H. (2000) An animal model of neuropathic pain employing injury to the sciatic nerve branches. *NeuroReport* 11, 657–661.

(29) Salomé, C., Salomé-Grosjean, E., Park, K. D., Morieux, P., Swendiman, R., DeMarco, E., Stables, J. P., and Kohn, H. (2010) Synthesis and anticonvulsant activities of (R)-N-(4'-substituted)benzyl 2-acetamido-3-methoxypropionamides. *J. Med. Chem.* 53, 1288–1305.

(30) Swinyard, E. A. (1969) Laboratory evaluation of antiepileptic drugs: review of laboratory methods. *Epilepsia* 10, 107–109.

(31) Paverello, P., Bonsignori, A., Caccia, C., Amici, R., McArthur, R. A., Fariello, R. G., Salvati, P., and Varasi, M. (1999) Sodium channel activity and sigma binding of 2-aminopropanamide anticonvulsants. *Bioorg. Med. Chem. Lett.* 9, 2521–2544.

(32) Fariello, R. G., McArthur, R. A., Bonsignori, A., Cervini, M. A., Maj, R., Marrari, P., Pevarello, P., Wolf, H. H., Woodhead, J. W., White, H. S., Varasi, M., Salvati, P., and Post, C. (1998) Preclinical evaluation of PNU-151774E as a novel anticonvulsant. *J. Pharmacol. Exp. Ther.* 285, 397–403.

(33) For comparable procedures for resolving stereoisomers, see the following: (a) Weisman, G. R. (1983) In *Asymmetric Synthesis-Analytical Methods* (Morrison, J. D., Ed.), Vol. 1, pp 153–171, Academic Press, New York. (b) Parker, D., and Taylor, R. J. (1987) Direct <sup>1</sup>H NMR assay

of the enantiomeric composition of amines and β-amino alcohols using O-acetyl mandelic acid as a chiral solvating agent. *Tetrahedron* 43, 5431–5456.

(34) Wang, Y., Brittain, J. M., Jarecki, B. W., Park, K. D., Wilson, S. M., Wang, B., Hale, R., Meroueh, S. O., Cummins, T. R., and Khanna, R. (2010) In silico docking and electrophysiological characterization of lacosamide binding sites on collapsin response mediator protein-2 identifies a pocket important in modulating sodium channel slow inactivation. *J. Biol. Chem.* 285, 25296–25307.

(35) Rudy, B. (1978) Slow inactivation of the sodium conductance in squid giant axons. Pronase resistance. *J. Physiol.* 283, 1–21.

(36) Hodgkin, A. L., and Huxley, A. F. (1952) The dual effect of membrane potential on sodium conductance in the giant axon of Loligo. *J. Physiol.* 116, 497–506.

(37) Bean, B. P. (2007) The action potential in mammalian central neurons. *Nat. Rev. Neurosci.* 8, 451–465.

(38) Do, M. T., and Bean, B. P. (2003) Subthreshold sodium currents and pacemaking of subthalamic neurons: modulation by slow inactivation. *Neuron* 39, 109–120.

(39) Vilin, Y. Y., and Ruben, P. C. (2001) Slow inactivation in voltage-gated sodium channels: molecular substrates and contributions to channelopathies. *Cell Biochem. Biophys.* 35, 171–190.

(40) Catterall, W. A. (2002) Molecular mechanisms of gating and drug block of sodium channels. *Novartis Found. Symp.* 241, 206–218, discussion 218–232.

(41) Leach, M. J., Marden, C. M., and Miller, A. A. (1986) Pharmacological studies on lamotrigine, a novel potential antiepileptic drug: II. Neurochemical studies on the mechanism of action. *Epilepsia* 490–497.

(42) Woodbury, D. M. (1980) Phenytoin: proposed mechanism of anticonvulsant action. *Adv. Neurol.* 27, 447–471.

(43) Barnes, S., and Hille, B. (1988) Veratridine modifies open sodium channels. *J. Gen. Physiol.* 91, 421–443.

(44) Ulbricht, W. (1998) Effects of veratridine on sodium currents and fluxes. *Rev. Physiol., Biochem., Pharmacol.* 133, 1–54.

(45) Wang, Y., and Khanna, R. (2011) Voltage-gated calcium channels are not affected by the novel anti-epileptic drug lacosamide. *Transl. Neurosci.* 2, 13–22.

(46) Decosterd, I., Allchorne, A., and Woolf, C. J. (2004) Differential analgesic sensitivity of two distinct neuropathic pain models. *Anesth. Analg.* 99, 457–463.

(47) Filatov, G. N., and Rich, M. M. (2004) Hyperpolarized shifts in the voltage dependence of fast inactivation of Nav1.4 and Nav1.5 in a rat model of critical illness myopathy. *J. Physiol.* 559, 813–820.

(48) Rich, M. M., and Pinter, M. J. (2003) Crucial role of sodium channel fast inactivation in muscle fibre inexcitability in a rat model of critical illness myopathy. *J. Physiol.* 547, 535–566.

(49) Jarecki, B. W., Sheets, P. L., Jackson, J. O., and Cummins, T. R. (2008) Paroxysmal extreme pain disorder mutations within the D3/S4-S5 linker of Nav1.7 cause moderate destabilization of fast inactivation. *J. Physiol.* 586, 4137–4153.

(50) Backonja, M. M. (2002) Use of anticonvulsants for treatment of neuropathic pain. *Neurology* 59, S14–S17.

(51) Challopalli, V., Tremont-Lukats, I. E., McNicol, E. D., Lau, J., and Carr, D. B. (2005) Systemic administration of local anesthetic agents to relieve neuropathic pain. *Cochrane Database Syst. Rev.* CD003345.

(52) Hildebrand, M. E., Smith, P. L., Bladen, C., Eduljee, C., Xie, J. Y., Chen, L., Fee-Maki, M., Doering, C. J., Mezeyova, J., Zhu, Y., Belardetti, F., Pajouhesh, H., Parker, D., Arneric, S. P., Parmar, M., Porreca, F., Tringham, E., Zamponi, G. W., and Snutch, T. P. (2011) A novel slow-inactivation-specific ion channel modulator attenuates neuropathic pain. *Pain* 152, 833–843.

(53) Vissers, K. C. P., Geenen, F., Biermans, R., and Meet, T. F. (2006) Pharmacological correlation between the formalin test and the neuropathic pain behavior in different species with chronic constriction injury. *Pharmacol., Biochem. Behav.* 84, 479–486.

(54) Wang, Y., Brittain, J. M., Wilson, S. M., Hingtgen, C. M., and Khanna, R. (2010) Altered calcium currents and axonal growth in Nf1 haploinsufficient mice. *Transl. Neurosci* 1, 106–114.

(55) Taylor, A. L., and Hewett, S. J. (2002) Potassium-evoked glutamate release liberates arachidonic acid from cortical neurons. *J. Biol. Chem.* 277, 43881–43887.

(56) Kuo, C.-C., and Bean, B. P. (1994) Slow binding of phenytoin to inactivated sodium channels in rat hippocampal neurons. *Mol. Pharmacol.* 46, 716–725.